The International Journal of Advanced Manufacturing Technology (2023) 124:2011–2036
https://doi.org/10.1007/s00170-022-10561-0

CRITICAL REVIEW

Heat-assisted incremental sheet forming for high-strength materials — a review

Weining Li[1] · **Moataz M. Attallah**[2] · **Khamis Essa**[1]

Received: 21 July 2022 / Accepted: 17 November 2022 / Published online: 8 December 2022

Abstract
Single-point incremental forming (SPIF) is a sheet forming technique that deforms sheet materials incrementally to a designated shape. The process has shown high ability to deform low-strength materials for good geometrical accuracy and formability at room temperature. Deforming high-temperature alloys, such as high-strength steels and Ti-6AI-4 V, requires integrated heat sources to increase the ductility of the metal sheets for deformation. However, the integration of heating results in unpredictable thermal behaviours and impacts the formability, geometric accuracy, thickness distribution and surface quality. Considerable research efforts have invented different heating methods and designed novel tools and analytical modelling to resolve the limitations. The current challenge remains improving the localised and stable heating, functional tool design to reduce the thermal expansion and friction at the tool-surface contact area and the analysis of relationship between thermal and mechanical effects. This study aims to review the heating-assisted SPIF systems for high-strength alloy sheets to solve the current limitations. The method includes analysis of heating systems, tool, tool path design, lubricants and macro- and micro-numerical analyses. Additionally, the study aims to correlate the microstructural properties to the mechanical behaviours and subsequent effects on forming force, strain, springback, geometrical accuracy and surface quality.

Keywords Heating-assisted single-point incremental forming · High-strength alloys · Tools · Tool path · Lubricant · Numerical analysis · Microstructural analysis

1 Introduction

Conventional sheet-forming processes are normally established in complex and expensive tool system designs fixed for limited designated geometry and only economically feasible for mass production. The global challenge in the manufacturing industry includes developing flexible and economical forming processes to produce sheet materials in complicated geometry for rapid prototyping. Single-point incremental sheet forming (SPIF) is a new class forming process which can complete the objectives. SPIF has undergone development in recent years and refers to a die-less sheet forming process and excels in forming complex shapes or rapid prototypes using universal tools.

SPIF is a die-less incremental sheet forming (ISF) process which provides maximum flexibility in the sheet metal forming category. The workpiece is clamped by the edges rigidly without any supporting dies underneath and applicable to approach the deforming tool for complex forming shapes. The process is applicable for metal alloy and polymer sheets, and the tool path can be generated from the computer-aided design (CAD), which shows its suitability for the majority of complex forming shapes.

SPIF shows a significant improvement in formability as the nature of the die-less forming process provides maximum flexibility for the forming tool movements. For instance, the studies [1, 2] investigated the improvement in formability and geometric accuracy for low-strength alloy sheets (aluminium, magnesium, copper). Furthermore, Zhan et al. [3] investigated single-pass friction stir–assisted incremental sheet forming (FS-ISF) which is

✉ Khamis Essa
k.e.a.essa@bham.ac.uk

Weining Li
w.li.3@bham.ac.uk

Moataz M. Attallah
m.m.attallah@bham.ac.uk

[1] Mechanical Engineering, University of Birmingham, Edgbaston, Birmingham B15 2TT, UK

[2] School of Metallurgy and Materials, University of Birmingham, Edgbaston, Birmingham B15 2TT, UK

able to improve the formability of aluminium alloy sheets. And Yan et al. [4] have studied the multi-stage tool path which successfully reduced the geometric inaccuracy and processing time. Other studies [5–8] also applied the forming process on polymers (polyvinyl chloride (PVC), polypropylene (PP), polyoxymethylene, polyethylene (PE), polyamide (PA), polycarbonate (PC) and polyethylene terephthalate (PET)) by modifying the tool path and tool design to achieve high formability with reduced fracture risk. According to the study by Jeswiet et al. [9], various axisymmetric forming structures can be deformed with high accuracy. Furthermore, Panjwani et al. [10] and Sousa [11] proved that the formability of SPIF can be expandable to both axisymmetric and non-axisymmetric forming shapes using specified tool path. The studies by Ben Said [12] and Liu [13] have reviewed the processing and modelling of current SPIF technology and proposed that the integration of heating source reserves future potential to improve the formability of high temperature materials; however, the following limitations have to be covered during the process.

Although SPIF can successfully deform low-strength materials since low forming force is needed, the current challenge revolves around integrating the heating source on high-temperature materials, such as titanium, nickel or steel, to increase the ductility of material sheets. Christopher et al. [14] have produced apparatus comprises a platform, stylus and a heating system to provide localised heating to the material and achieve a reduction of material forming force, which can be considered as a significant improvement in metal forming work to further improve the applicable materials. The previous study by Lu et al. [15] investigated that tool rotation induced vibration heating to the AZ31 magnesium sheets; the tool-surface friction induced localised heating successfully, generated localised heating to the workpiece and increased the ductility of material. Another study by Al-Obaidi et al. [16] investigated the electric-assisted SPIF on high-strength steel sheets which presented localised heating to the workpiece which successfully reduced the forming force and achieved better formability. Göttmann et al. [17] investigated the laser heating–assisted SPIF on Ti-6Al-4 V which revealed high-precision localised heating to the workpiece and relatively constant heating temperature to provide high geometric accuracy. However, the findings also indicate incredible springback, pronounced wear tracks on the surface and uneven thickness distribution. To overcome the limitations, previous research [18, 19] proposed ball-roller tools and multi-axis fixtures to produce a pronounced friction reduction during the process and enable a significant increase in wall angle to improve the formability. The studies [20–23] proposed mathematical methods to compensate the tool path, and studies [24–27] applied artificial neural networks to study and improve the tool path plan to reduce the error from springback and prediction of temperature distribution during the process.

Although significant improvements have achieved in these studies, the equipment for heating sources is expensive and requires external safety measurements. The pronounced wear tracks and springback caused by the heating source are not fully solved. Thus, future improvements are required in this field to improve the geometric accuracy, surface quality, formability and a reduction in production cost.

This paper reviewed the recent improvements of SPIF on high-strength materials including the heating methods, forming tools, lubricant, tool path planning, numerical simulation and microstructure analysis. The deformation mechanism, accuracy, thickness, formability and surface roughness were analysed and correlated with the microstructure revolution. Furthermore, the microstructure evaluation was linked with the relevant numerical simulation and mechanical properties to analyse the effects from heating temperature, friction and inaccuracy compensation from tool path. Each analytical parameter was summarised at the end to provide the advantages and limitations for following users to determine regarding their specific process.

2 Heat-assisted single-point incremental forming

To increase the formability and geometric accuracy of conventional SPIF process for high-strength materials, heating sources represents a critical step to reduce the high forming force during the process. The commonly used heating sources in SPIF processes can be divided into five categories: friction stir, ultrasonic vibration, electric heating, laser heating and induction heating methods. Each heating method indicates advantages and limitations in the forming process and considerable future improvements.

2.1 Friction stir–assisted single-point incremental forming

Friction stir–assisted single-point incremental forming (FSSPIF) constitutes a simple heat-assisted SPIF process where the localised temperature can be applied to the workpiece at the deformation zone between the rapid tool movement and the contact workpiece. Giuseppina et al. [28] experimentally and numerically studied the temperature by friction during the FSSPIF and the parameter effects on the temperature distribution on the sheet material, which proved that the generated temperature is able to deform titanium alloys. However, a pronounced wear was detected on the deformed surface. Liu [29] applied FSSPIF to produce designated shapes on 1.5 mm AA7075-O sheets with different rotation tool speeds from 3000 to 7000 rpm,

which results in a temperature up to 140 °C to increase the ductility of materials and achieve a reduction in forming force to improve the formability.

However, this heating-assisted SPIF lacks stability and proves insufficient for high-strength materials. As shown in Fig. 1 [30], on the investigation of friction stir SPIF on 1 mm Ti-6Al-4 V sheets, which resulted in pronounced geometric inaccuracy, cracks, wear marks and significant tool wear have been reported as a rotation of 2000–3000 rpm with a temperature range from 400 to 460 °C. Ambrogio and Gagliardi [31] applied a rotation speed of 5000 rpm to Ti-6Al-4 V sheets, which achieved a temperature up to 600 °C. However, the generated temperature cannot be maintained constantly, resulting in unpredictable springback and reduced surface quality. This result indicates that FSSPIF is not reliable to produce high accuracy and surface quality products for high-strength materials due to its non-constant temperature increase.

2.2 Ultrasonic vibration single-point incremental forming

Ultrasonic vibration single-point incremental forming (UVSPIF) has developed from the UV stamping, drawing, drilling, extrusion and hydroforming operations of metal alloys and polymers [32–38] to enhance the forming limits by applying vibrated-localised deformation to the forming tool. The standard UVSPIF process is illustrated in Fig. 2a [39], and the measured forming force reduction is illustrated in Fig. 2b [39]. It can be noticed that the average forming force was reduced around 500 N during UVSPIF of pure titanium bimetal sheet. Baghlani et al. [34] successfully applied a

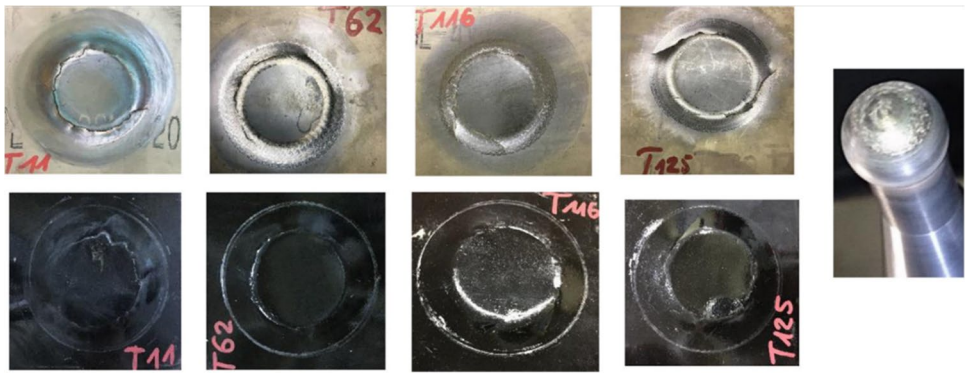

Fig. 1 Results obtained from the friction stir SPIF of Ti-6Al-4 V sheets [30]

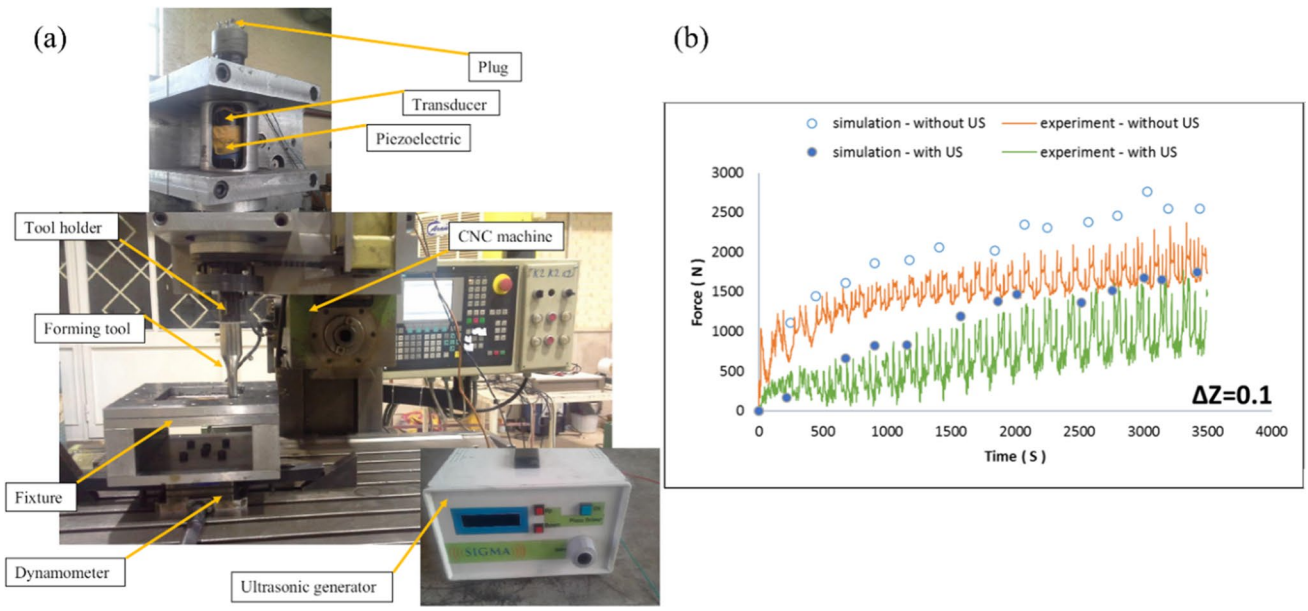

Fig. 2 Experimental setup of UVSPIF process. **a** Illustration of UVSPIF, **b** measured forming force from the UVSPIF process. US, ultrasonic forming force [39]

high-frequency vibration feed rate in the drilling process to increase the rotational speed of the tool, and the temperature can be transferred to the workpiece by contacting; the results indicated a strong reduction in forming force during the process of Inconel 738LC superalloy. Cheng et al. [40] applied UV to deform Al 7075 alloy sheets in the SPIF and two-point incremental forming (TPIF) processes at 20 kHz oscillating frequency. The study commented that there is a significant reduction of applied forming forces during both processes which successfully increased the ductility of the materials and improved the formability accordingly. Due to the energy transfer to membrane vibration, the magnitude of force reduction in SPIF proves relatively lower than TPIF. Bai et al. [41] applied static pressure support in UVSPIF to study the forming force's relevance to the static pressure. By increasing the frequency to approximately 30 kHz, the pressure produces a sufficient grain size reduction of the 1-mm AL1060 sheets to increase the material ductility. The study by Sun et al. [42] proposed that the UVSPIF process could reduce the springback and waviness feature to improve the geometric accuracy and surface quality to improve 2-mm AA-5052 sheets compared with the conventional SPIF process. Cheng et al. [43] commented that the forming force of UVSPIF of AA1050-O alloy sheets can be reduced by 66.7% using a 10-μm vibration amplitude.

Recently, Sakhtemanian et al. [39] studied UVSPIF on low carbon steel/commercially pure titanium bimetal alloy sheets. The findings show that the localised temperature reached approximately 250 °C and a reduction of vertical applied forming force from 3000 to 1000 N (average reduction). Furthermore, the study detected a recrystallisation (DRX) process and followed flow stress decrease. The phenomenon indicates further improvements in formability if higher temperature can be applied. However, the study also proposed that the temperature induced by UV is unstable which results in uncontrollable forming force. The unstable temperature induced insufficient microstructure evolution and unpredictable straining effects which may result in high risk of crack especially for high-strength materials.

2.3 Electric heating–assisted single-point forming

To further increase the temperature for heat-assisted SPIF systems for high-strength materials, the studies [44–46] established analytical models to investigate the heating and deformation mechanism for the electric heating–assisted SPIF process. Meier and Magnus [47] and Möllensiep et al. [48] developed direct current (DC) to the robotic arm–controlled tools to direct a temperature of 600 to the steel metal sheets. The study reported a significant reduction in the forming force in producing the flexible and accurate forming shape for 1-mm DC04 steel. Other studies [49, 50] investigated the electric-heating SPIF of Ti-6Al-4 V sheets by introducing a DC power to the interface of the Ti-6Al-4 V sheet and tool to form a simple DC closed circuit, as shown in Fig. 3. According to Joule's law, a flowing DC current from tool to workpiece generates heat and raises temperature and flux through the area. To ensure the safety, tool and workpiece are insulated to allow a restricted area for flux flow. The electric heating of Ti-6Al-4 V sheets for various target temperatures produces different results. For instance, Fan et al. [51] achieved a relatively stable temperature distribution at 500 °C. The obtained surface quality result, shown in Fig. 4a, reveals a significant Joule heat effect on the inner surface of the workpiece. Another study by Ao et al. [52] increased the temperature to 820 °C using a high-power generator to provide large energy to Ti-6Al-4 V sheets. However, the formed shapes were not optimal; as shown in Fig. 4b, large cracks, pronounced

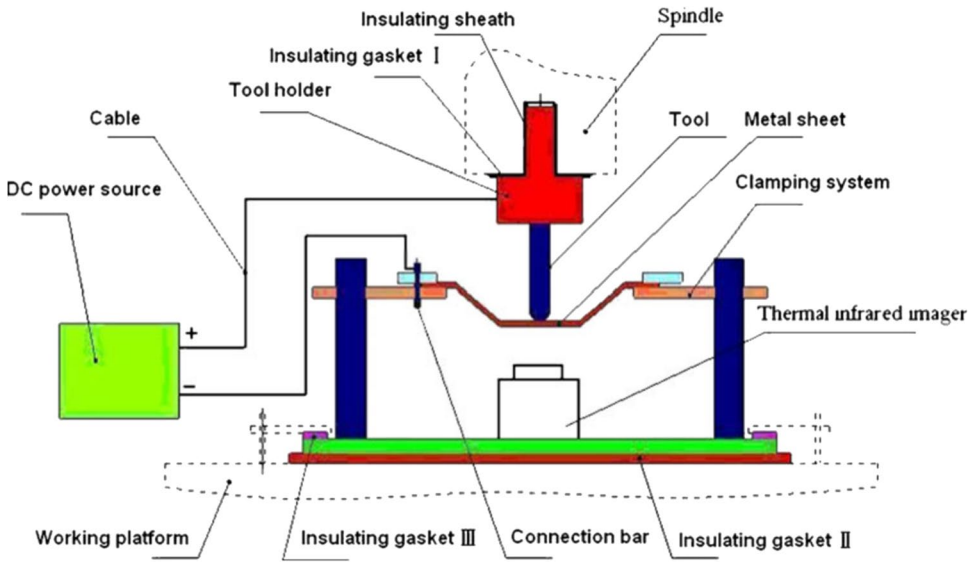

Fig. 3 Illustration of electric heating SPIF system [49]

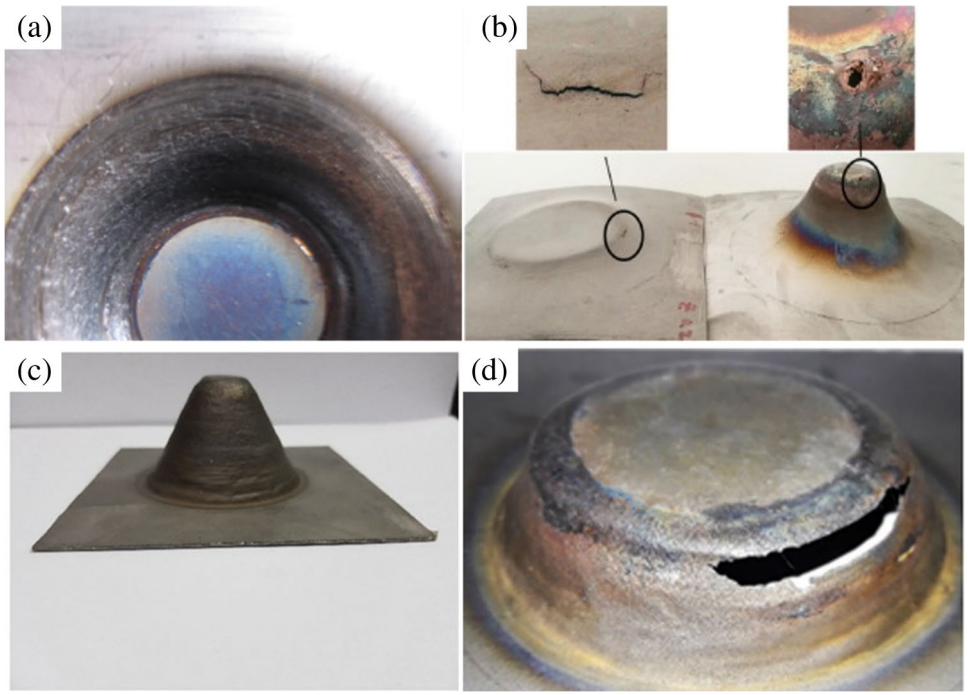

Fig. 4 Obtained surface quality results. **a** Joule heating effect on inter-surface [51], **b** cracks on outer surface [52], **c** outer surface [50], **d** cracks on outer surface [53]

springback and burning holes were detected. This result can be attributed to the unstable temperature distribution and friction along the process, which produced electric sparks at tool-workpiece contact area and induced unpredictable deformation along the tool path of the workpiece. Vahdani et al. [50] maintained the forming temperature at 690 °C, which successfully achieved an increase of formability where the wall angle increased to 60 ° and reached a base depth of 58 mm, as shown in Fig. 4c. Vahdani et al. [53] induced a temperature of 750 °C to Ti-6Al-4 V, AA6061 aluminium and DC01 steel sheets, which also revealed a pronounced Joule heating effect on the formed shapes and large cracks appeared, which indicated such an effect's proportionality to the temperature: The higher temperature induces greater Joule heating effect.

In summary, electric heating–assisted SPIF represents an acceptable method to process high-temperature alloy sheets, which can produce high formability. However, the flux of current induces the temperature on the whole workpiece and temperature is not maintained constantly between the contact area under the forming tool and other areas of the workpiece. Furthermore, the flux of current also induces a significant Joule heating effect according to the temperature, resulting in noticeable springback, cracks, wear tracks and oxidations. Thus, a constant high-temperature localised heating method is required to heat the contact area between the forming tool and workpiece.

2.4 Laser heating–assisted single-point incremental forming

In order to provide precise and localised elevated temperature to the predefined tool path in hot SPIF operations, Duflou et al. [54] proposed laser heating to provide accurate and localised elevated temperature to the predefined tool path in hot SPIF operations and deform 1.25-mm Al 5182 sheet metals. By adjusting the power of the beam to 500 W, the temperature can remain constant up to 350 °C. Compared with the room temperature SPIF, the forming force was reduced approximately to 50%, and the forming angle increased from 32 to 56 °. However, the relative lower temperature did not reduce the springback during the process, and heating on the surface reduced the surface quality. Lehtinen et al. [55] studied laser heating SPIF on 0.75 mm DC04 steel using a 1-kW fibre laser. Although the study investigated laser heating on high-strength sheet metal, the surface quality could not compare with that produced under room temperature, as shown in Fig. 5a, b, where pronounced heating wear and minor cracks appeared on the surface with heating (Fig. 5b) and the room temperature product (Fig. 5a) provided a smooth surface without noticeable wear and cracks.

Göttmann et al. [56] proposed a high-power (10 kW) fibre laser heating–assisted SPIF system and developed in the study by Göttmann et al. [17] for 1.5-mm Ti-6Al-4 V sheets, as shown in Fig. 6a, b, where the laser spot system

has been attached to the tool to allow a sync movement. The laser heating system uses beam shaping optics and displacement to direct the laser beam to the advanced area of the tool to provide rapid heating. The temperature can be maintained at 400 °C to provide localised heating on the workpiece surface. However, the obtained surface quality does not reach the required levels. The laser beam heating dissipates the lubricant rapidly in advance of the tool, thus resulting in a large area of scratches between the surface and tool. Findings also show that the material's particles have produced from the surface and left a large volume of the wear debris on the surface, as shown in Fig. 7a. Removing the coating from the tool due to the high temperature results in a high adhesion of lubricant and wear debris to the tool, which may affect the geometric accuracy and surface quality.

2.5 Induction heating–assisted single-point incremental forming

Compared with the discussed heating methods in previous sections, induction heating–assisted SPIF can provide high temperatures and localised heating to the workpiece with relatively low-cost equipment and higher surface quality. Al-Obaidi et al. [16] proposed a tool-heater synchronised induction heating–assisted SPIF system, as shown in Fig. 8. The induction heating coil is positioned underneath the

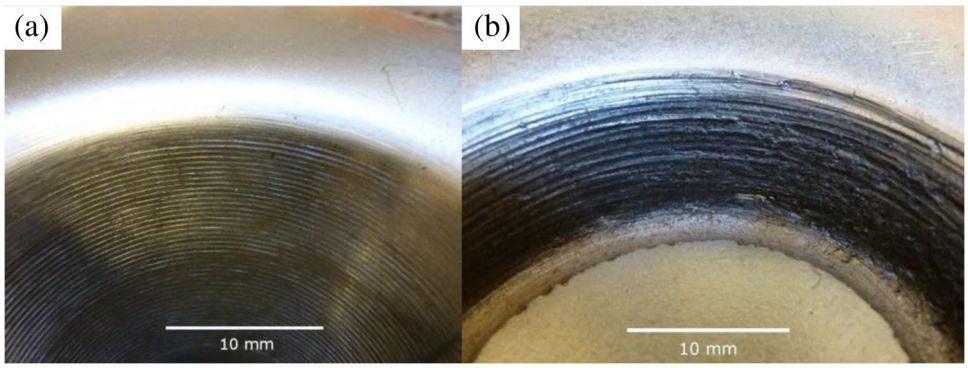

Fig. 5 Surface quality of final formed workpiece. **a** Without heating, **b** with heating [55]

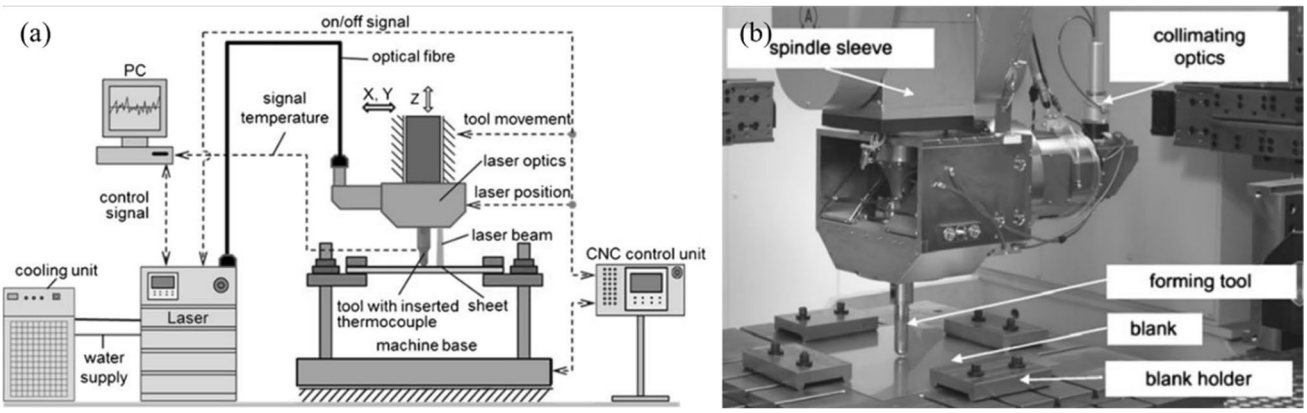

Fig. 6 Laser heating SPIF system. **a** Working mechanism [56], **b** experimental setup [17]

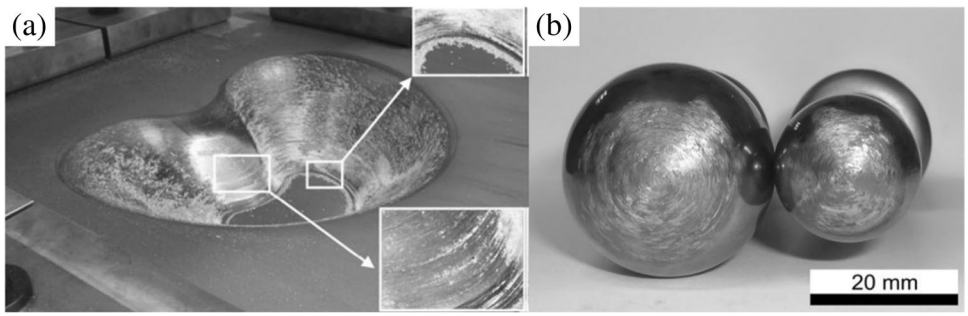

Fig. 7 Surface quality and tool wear. **a** Surface quality of formed workpiece, **b** tool wear on different tool tip diameters [17]

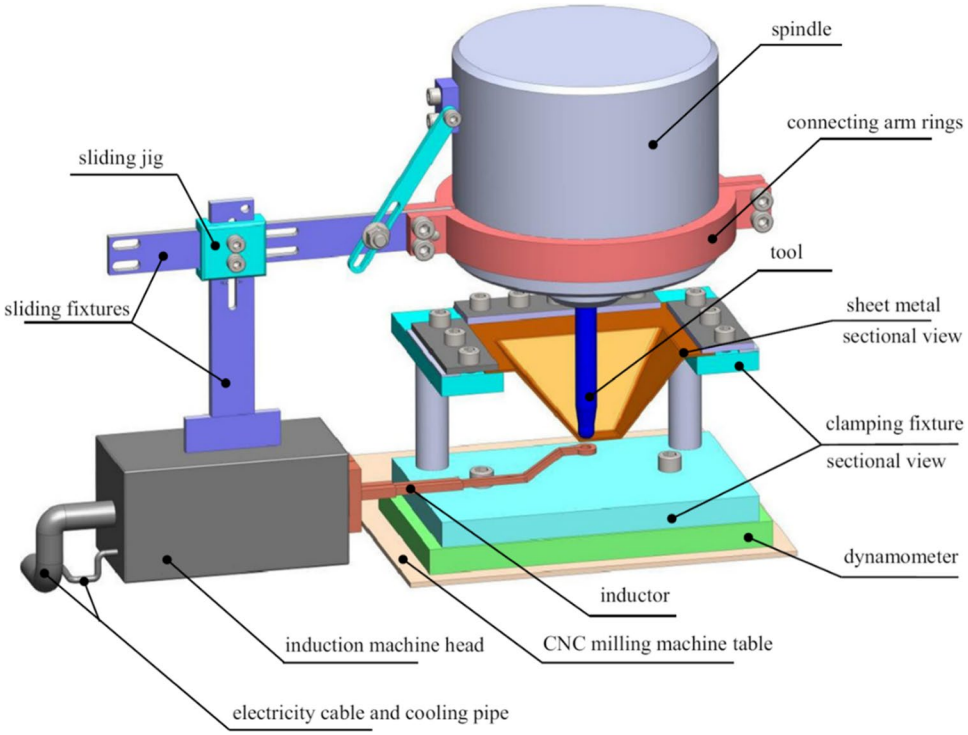

Fig. 8 Illustration of induction heating–assisted SPIF system [16]

workpiece and connected to the mounting of as the forming tool to synchronise movements. The study investigated the forming process for 1.6-mm DP 980 steel dual-phase metal sheets. Wall angles of 45 °, 55 ° and 60 ° underwent testing at temperatures of 785 °C, 790 °C and 800 °C with a tolerance of 30 °C. The obtained results indicate a dramatic improvement in geometric accuracy compared with that achieved under the room temperature, which cannot produce a complete forming shape. The study also observed the improved geometric accuracy at the region with constant induction power, where higher power indicated a higher reduction in springback. Such a situation means higher temperature reduces more forming forces and results in better ductility to achieve higher geometric accuracy. Al-Obaidi et al. [57] further investigated the induction heating-assisted SPIF on 1.2-mm HCT 980C steel to achieve a wall angle of 70 °. The results reveal that the forming forces can be decreased to 66.7% using 5 kW power to provide localised heating at 750 °C to the workpiece.

Ambrogio et al. [58] investigated an induction heating SPIF process on 1-mm Ti-6Al-4 V sheets for 600 °C and 700 °C with an additional cooling system. A tank of liquid nitrogen had been prepared to spray the tool-surface contact area at different phases of the process. According to the results, the cooling process significantly improved the geometric accuracy. Compared with friction and electric heating–assisted SPIF, induction heating reserves less safety measurements and applicable to integrate with external features to improve the process quality. Such heating method is able to provide a localised heating to the tool-workpiece contact area to increase the geometric accuracy and reduce the lubricant dissipation on the surface; the comparison between room temperature, electric heating and induction heating is shown in Fig. 9a–c.

The induction heater has a relatively lower cost and simple setup compared with the previously discussed heating-assisted SPIF systems, and the product quality is better achieved. The localised and accurate heating results in improved geometric accuracy and formability. However, the surface quality can be further improved. As shown in Fig. 10a, b, by applying same MoS_2 lubricant and closed heating temperature on Ti-6Al-4 V sheets, the electric heating–assisted SPIF product [53] in Fig. 10a revealed pronounced wear and cracks on the formed surface, and the induction heating–assisted SPIF product [59] in Fig. 10b produced better surface quality. The study by induction heating commented that the lubricant dissipation is according to the temperature, while higher temperature (around 700 °C) significantly increased dissipation from early stage of the process. To reduce such effects, Li et al. [60] applied a water-cooling channel tool to assist a flow of liquid lubricant to reduce the temperature at tool-surface contact area. Such an approach is adjustable and able to produce stable heating temperature throughout the process to induce equiaxed microstructural evolution and maintain a constant DRX process.

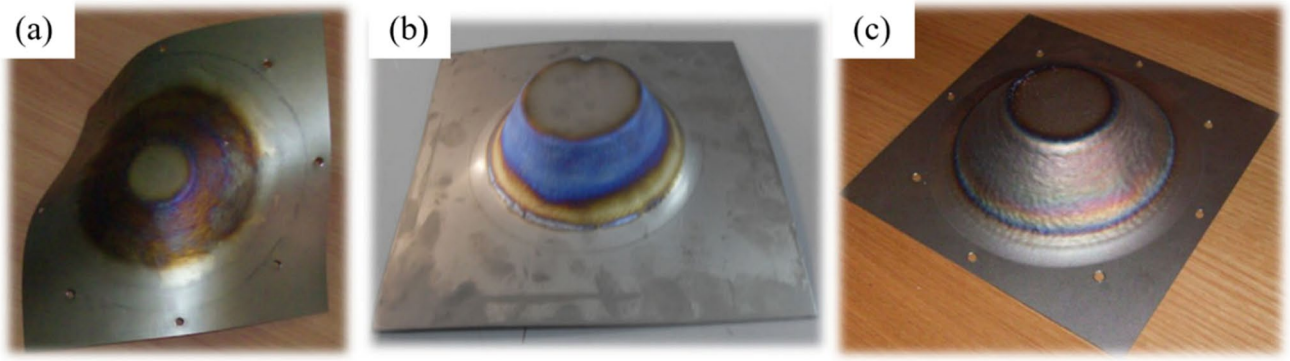

Fig. 9 Observed geometric profile. **a** Room temperature, **b** electric heating, **c** induction heating with cooling [58]

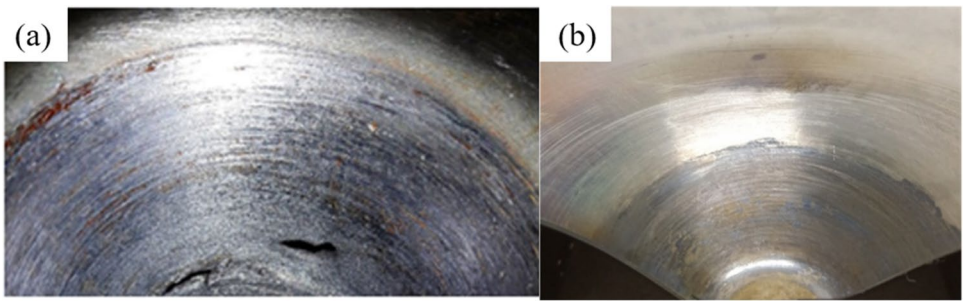

Fig. 10 Comparison of surface quality. **a** Electric heating–assisted SPIF [53], **b** induction heating–assisted SPIF [59]

2.6 Summary of heat-assisted single-point incremental sheet process

Heat-assisted SPIF processes have significantly improved the deformation of high-strength materials. However, due to the regional or localised heating methods, numerous issues require addressing, including temperature dominant stress–strain effects on the formability and geometric accuracy, wear debris and lubricant dissipation effects on the surface quality, constant and accurate heating temperature to the workpiece and the need to design efficient tools to reduce the friction at the contacting area. Table 1 presents the summary of heating methods and relevant findings from each heat-assisted SPIF process.

3 Tool design

The forming tool has critical effects on forming shapes, geometric accuracy and surface quality. The conventional tools have stable and sufficient performance for the SPIF process of low-strength materials. However, conventional tools were unable to provide sufficient performance for high-strength materials, especially in the heat-assisted SPIF process. This section compares the conventional tools with ball-roller tools' performance in formability, geometric accuracy and surface quality.

3.1 Conventional tools

In the heat-assisted SPIF process for high-strength materials, the tools must take the pronounced thermo-mechanical deformation from the process, preventing the thermo-expansion from the temperature and adhesion of lubricant during the incremental steps. The conventional tools in SPIF have a hemisphere shape with a diameter from 5 to 20 mm, according to the experimental designs. Figure 11 presents a series of tools designed in the hemisphere and flat shapes with different tooltip diameters according to the wall angle and step size. For heat-assisted SPIF operations, conventional tools did not provide high-performance levels in terms of surface quality and geometric accuracy. Figure 12 illustrates the investigation by Vahdani et al. [53] of the electric heating–assisted SPIF on Ti-6Al-4 V sheets at 750 °C. The outer shape presented an uneven geometry in forming thickness and pronounced wear, and abrasive adhesion of lubricant appeared on the inner workpiece and tool, which indicated the low functioning endurance of conventional tools during the heat-assisted SPIF. Kumar et al. [62] investigated the forming limits of conventional tools (hemisphere and flat), as shown in Fig. 13a, b, where R_1 has a tool diameter of 3.76 mm and R_2 has a tool diameter of 7.52 mm with a side diameter (tool corner) of 1.4 mm. The study found that the hemisphere tool achieved higher formability than flat tools as

Table 1 Summary of different heat-assisted SPIF processes

Heating methods	Materials	Advantages	Limitations	Refs
Friction stir	AA7075-O, Ti-6AL-4 V	- Low cost - Localised heating by friction - Efficient for low-strength materials - Temperature up to 600 °C	- Passive heating method - Temperature is uncontrollable - Not efficient for high-strength materials - Not efficient enough to sufficiently reduce forming force - Significant springback and unfavourable surface quality for high-strength materials	Liu [29], Grün et al. [30], Ambrogio and Gagliardi [31]
Ultrasonic vibration	INCONEL 738LC, AL 7075, AL1060, AA-5052, AA1050-O, low carbon steel/commercially pure titanium bimetal alloy	- Low cost - Localised heating by ultrasonic vibration - Efficient for low-strength materials - Temperature can be reached at 250 °C	- Passive heating method - Temperature is uncontrollable - Not efficient for high-strength materials - Not sufficiently efficient to reduce forming force - Significant springback and unfavourable surface quality for high-strength materials - Low formability for high-strength materials	Baghlani et al. [34], Cheng et al. [40], Bai et al. [41], Sun et al. [42], Cheng et al. [43], Sakhtemanian et al. [39]
Electric heating	DC 04 steel, Ti-6Al-4 V	- Medium cost - Active heating method - Regional heating to the workpiece - Temperature is controllable from 400 to 750 °C - Efficient for high-strength materials	- Temperature is uncontrollable above 800 °C - Large Joule heating effects - Detectable springback and unfavourable surface quality - High percentage of product failures	Meier and Magnus [47], Fan et al. [51], Vahdani et al. [53], Ao et al. [52], Vahdani et al. [53], Möllensiep et al. [48]
Laser heating	Al 5182, DC 04 steel, Ti-6Al-4 V	- Active heating method - Localised heating - Temperature is controllable from 350 to 400 °C - Sustainable and constant heating support - High formability - Efficient for high-strength materials - Sufficient reduction in forming force	- High cost - Laser heating is not available for temperatures higher than 400 °C -Laser heating burns the surface and damages the surface quality - Rapid dissipation of lubricant - Complex experimental setup and safety measurements	Duflou et al. [54], Lehtinen et al. [55], Göttmann et al. [17], Göttmann et al. [56]
Induction heating	DC 04 steel, DP 980 steel, HCT 980C steel, Ti-6Al-4 V	- Low cost - Active heating method - Localised heating - Rapid and constant heat transfer - No limitation of temperature - Efficient for high-strength materials - Sufficient reduction in forming force - High formability	- Uneven localised temperature support to the workpiece - Rapid dissipation of lubricant - Significant wear - Detectable springback	Al-Obaidi et al. [16], Ambrogio et al. [58], Li et al. [59]

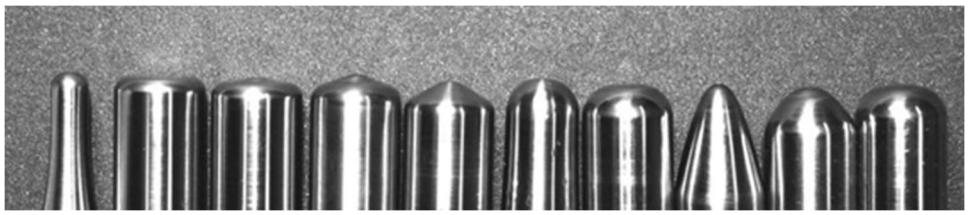

Fig. 11 Different tool shapes and dimensions [61]

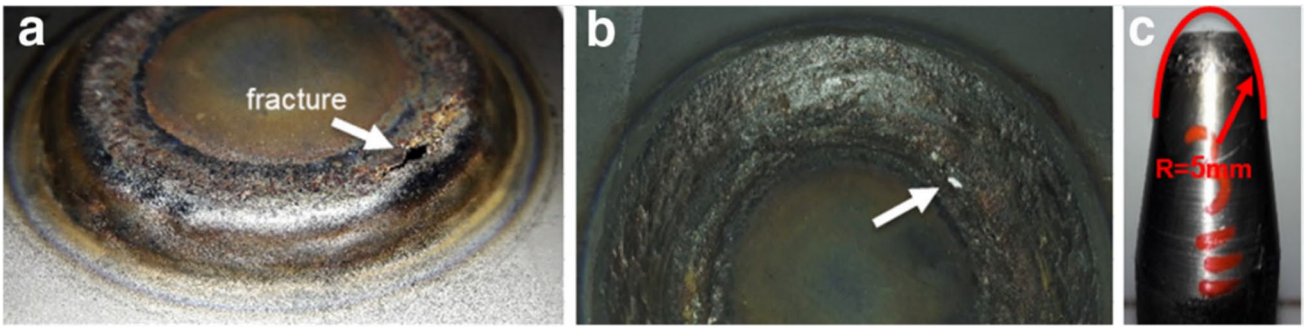

Fig. 12 Electric heating–assisted SPIF of Ti-6Al-4 V. **a** Outer surface, **b** inner surface, **c** tool tip wear [53]

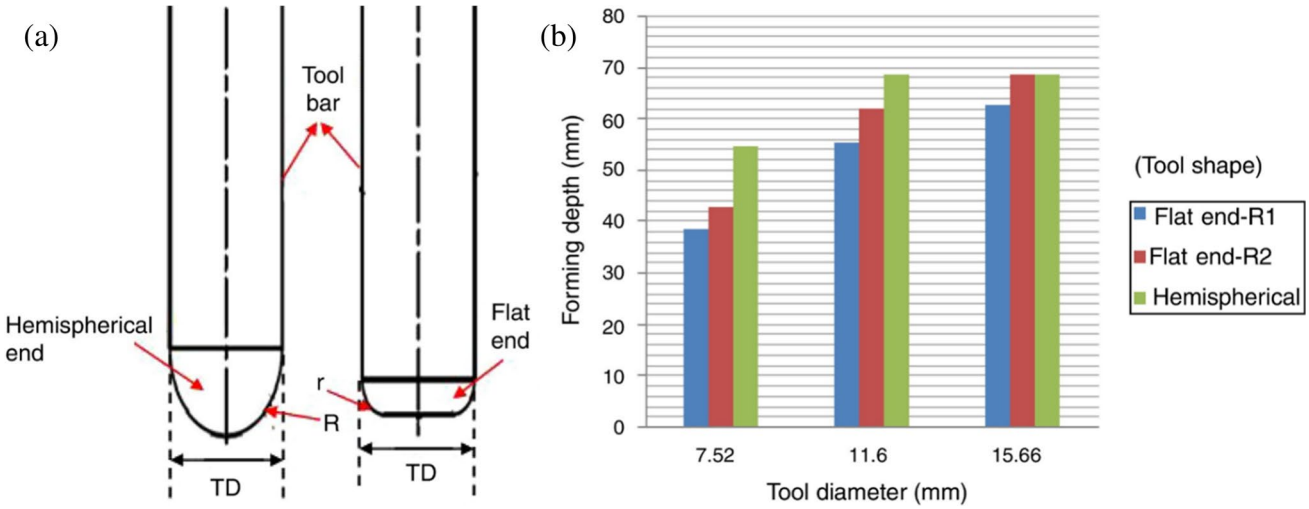

Fig. 13 Conventional tool and effects. **a** Tool shape and diameter, **b** effect of tool diameter on forming depth [62]

it increased the rounded surface reduces the contact to the workpiece. The flat tool surface able to produce more accurate geometric; however, the tool corner is increased to reduce the formability. The size of tool is relevant to the geometric accuracy and formability; smaller tool size is applicable to take smaller step size which is essential to produce more accurate geometry and complicated shapes. However, the lower contact area increased the forming force which increased the risk of cracking in forming of high in-depth shapes.

3.2 Ball-roller tools

Recently, ball-rolling tools have been designed to reduce the friction between the tool and workpiece, as shown in Fig. 14a, produced by Iseki [63]. The plane-strain deformation model in Fig. 14b reveals the approximation of strain distribution between the ball-roller tool and workpiece. The study proposed a relationship between the strain distribution by rolling tool and the forming geometry according to the ball-roller radius, wall angle and working depth. The proposed equations

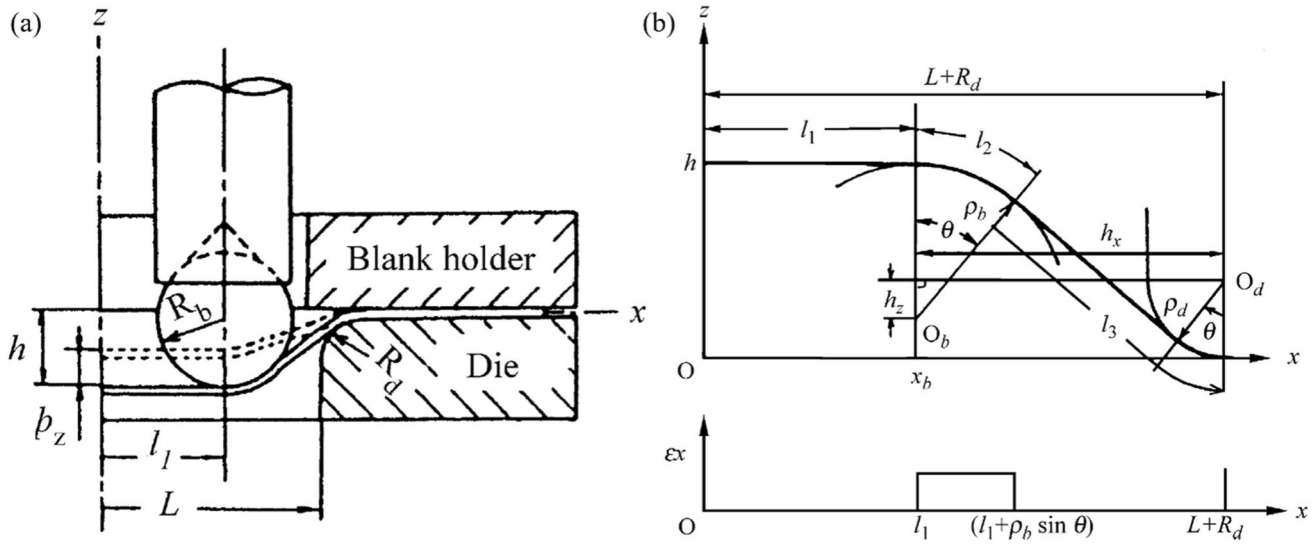

Fig. 14 Ball-roller tool and working mechanism. **a** Section view of the ball-roller tool, **b** plane-strain deformation of the ball-roller tool [63]

have been further validated in a study by Iseki and Naganawa [64]. The relationship can be expressed as follows:

$$\theta = \sin^{-1}\left[\frac{\rho_{\mathrm{b}} + \rho_{\mathrm{d}}}{\left(h_x^2 + h_z^2\right)^{1/2}}\right] - \tan^{-1}\left(\frac{h_z}{h_x}\right) \tag{1}$$

$$\rho_{\mathrm{b}} = R_{\mathrm{b}} + \frac{1}{2}t_0, \rho_{\mathrm{d}} = R_{\mathrm{d}} + \frac{1}{2}t_0 \tag{2}$$

$$h_x = L + R_{\mathrm{d}} - x_{\mathrm{b}}, h_z = \rho_{\mathrm{b}} + \rho_{\mathrm{d}} - h \tag{3}$$

$$l_1 = x_{\mathrm{b}}, l_2 = \rho_{\mathrm{b}}\theta \tag{4}$$

$$l_3 = h_x\cos\theta - h_z\sin\theta + \rho_{\mathrm{d}}\theta \tag{5}$$

where R_{b} denotes the ball radius, R_{d} denotes the die hole shoulder radius, θ denotes the contact angle, L denotes the die hole distance, h denotes the shell bulging height and x_{b} denotes the ball centre location. By applying the extended rule of contact arc l_2, uniform strains ε_x, ε_y, and ε_t on the x -direction can be expressed as follows:

$$\varepsilon_x = -\varepsilon_t = \ln\left[\frac{l_2}{L + R_{\mathrm{d}} - l_1 - l_3}\right], \varepsilon_y = 0 \tag{6}$$

Lu et al. [65] proposed a novel ball-roller tool design, as shown in Fig. 15a. The ball roller was attached to the tool body and controlled by a 3-axis CNC machine with the roller (Fig. 15b) always facing the workpiece. According to the study, a maximum 80 ° wall angle can be achieved, and the designed tool was able to apply the tool tip to the

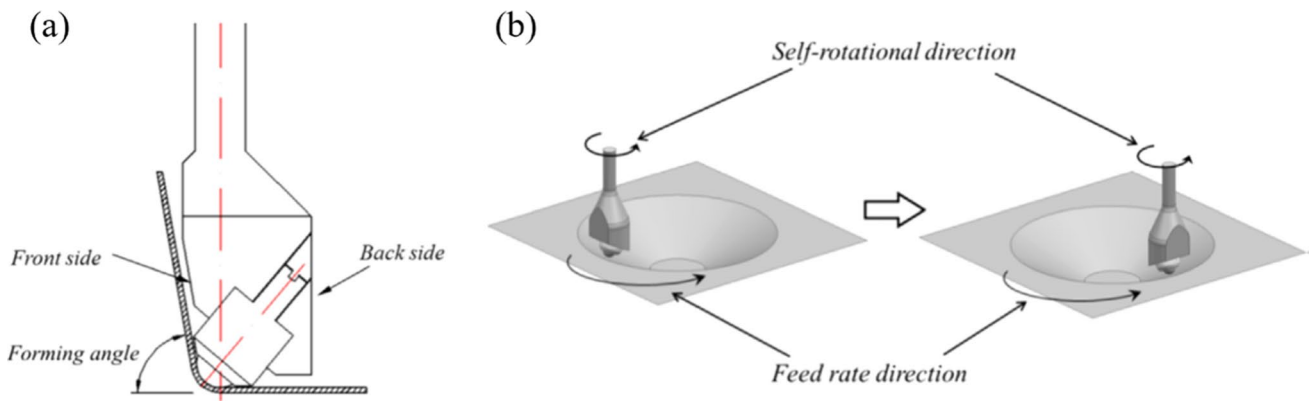

Fig. 15 Ball-roller tool and working mechanism. **a** Section view of ball-roller tool, **b** working mechanism in tool path [65]

forming wall to reduce the friction on the forming surface and achieved excellent geometric accuracy.

Naranjo et al. [66] investigated the tribological characterisation for oven-heated SPIF of Ti-6Al-4 V sheets at 200 °C, 300 °C and 400 °C. The ball roller is 10 mm in diameter, and all experiments were implemented without lubricant. The findings indicate that the adhesion of material increases with the rising temperature, which means a more pronounced rate of material adhesion at higher temperatures. The study also proposed that a tribo-layer can be observed as temperature increases due to heat diffusion.

To eliminate the adherence of material contamination and lubricant, Liu et al. [19] designed ball-rolling and wheel-rolling tools with inner water-cooling channel, as shown in Fig. 16a where the hollow tool with a water hole can be connected to the water tap, which induces water to cool down the steel ball roller. According to the study, the tool provided high-performance levels in the electric heating–assisted SPIF process for Ti-6Al-4 V at 500 °C. Similarly, another study by Li et al. [67] investigated on the proposed water-cooling ball-roller design in an induction heating–assisted SPIF process for Ti-6Al-4 V at 950 to 1100 °C. Figure 16b illustrates that the difference in this design is the orientation of the lubricating balls between the ball roller and the tool wall. To enhance the lubricating service from the water channel and prevent lock-on of the ball-roller during the process, double water holes and a baffle plug direct the liquid lubricant in and out to enable a pass-through process on the ball roller without affecting the temperature support. According to the study, the ball roller is made of IN 625 nickel alloy, with service temperature up to 980 °C. The geometric accuracy and surface quality can be obtained from Fig. 17a, b. The study applied a self-mixed liquid MoS_2 to pass through the ball roller to reduce the thermo-expansion during the process. The findings show that liquid lubricant helps reduce the springback

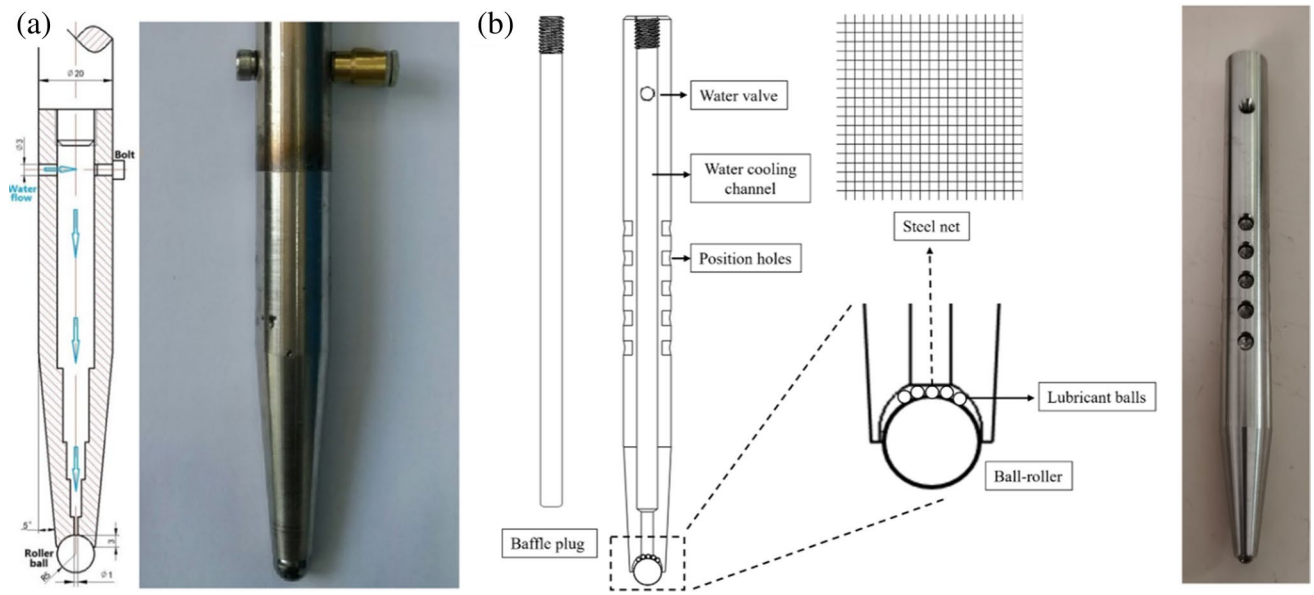

Fig. 16 Water-cooling ball-roller tool design. **a** Water-cooling ball-roller tool [19], **b** water-cooling ball-roller tool with assisted cooling design [67]

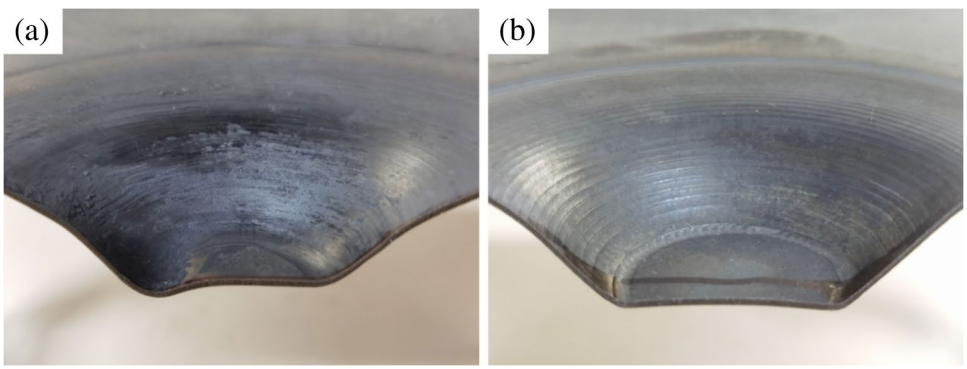

Fig. 17 Observed geometric profile and surface quality. **a** No liquid support, **b** continuous liquid lubricant support [67]

and enhances the surface quality where the wear marks and abrasive lubricant adhesion have been significantly removed.

3.3 Summary of tool design

The type, shape and tool diameter affect the formability, geometric accuracy and surface quality of forming shapes. The advantages and limitations of conventional tools and ball-roller tools for heat-assisted SPIF are presented in Table 2.

4 Tool path design

This section compares the effect of the contour and helical tool paths in the designs of forming shapes, geometric accuracy and surface quality. The tool path optimisation works, including compensation and machine learning models, will be discussed.

4.1 Contour and helical tool path

The tool paths for ISF processes are predefined by CAD/CAM software and implemented by CNC machines. According to the product shape, the tool path can have axisymmetric or non-axisymmetric designs. The tool path can be designed as a contour (z-level) profile or helical (spiral) profile, as shown in Fig. 18 [68]. The conventional tool path in Fig. 18a is in a contour profile where an accumulated step changes tool path to follow the tool motion to make steps according to the contour step. This tool path applies to any forming shapes, including axisymmetric or non-axisymmetric. However, the overlap of increment steps will leave a distinct mark on the deforming surface, as shown in Fig. 19a [69]. The helical tool path in Fig. 18b was able to overcome the limitation. Such tool path was developed by Skjoedt et al. [70] and applied in the study by Attanasio et al. [71]; the tool path uses an algorithm to produce a tool path to achieve the geometry without stopping for a step change. The algorithm can only produce an axisymmetric profile, and the starting and ending positions cannot be fully completed as the algorithm unable to complete a full circle tool path. As the forming shape illustrated in Fig. 19b, the helical tool path can provide high geometric accuracy and surface quality (no contour change); however, it is only limited to the axisymmetric forming shape due to its nature of mathematics calculation. The contour tool path is available for any shape, but the step change tool path affects the geometric accuracy and surface quality.

Table 2 Summary of tool design

Tool type	Advantages	Limitations
Conventional tool	- Low cost - Simple design - Different cap shape and size can be made to match process parameters	- Significant adhesion of removal materials and lubricant - Strong wear tracks - Low formability - High risk of cracking
Ball-roller tool	- Low wear tracks - Reduced contact area and rolling ball to reduce adhesion of materials and lubricants - The water-cooling system can be integrated to reduce the thermo-expansion of the ball roller - Ball rollers can be made of different materials to meet the thermo-mechanical strength for different sheet materials	- Complex design - High cost

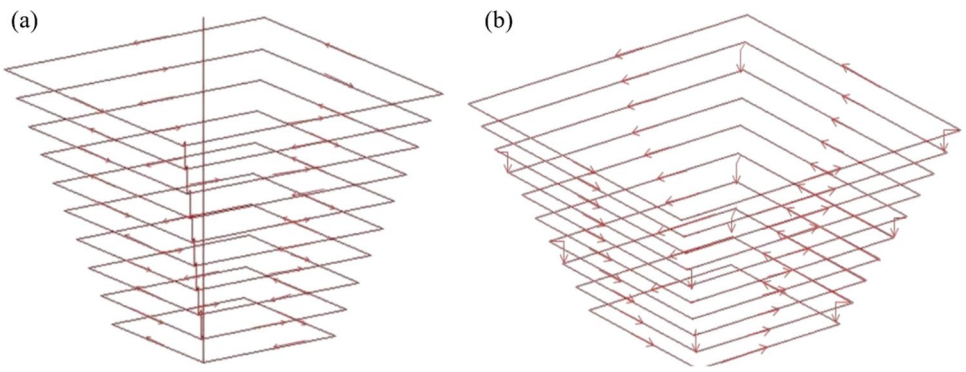

Fig. 18 Tool path design. **a** Contour (z-level) profile, **b** helical (spiral) profile [68]

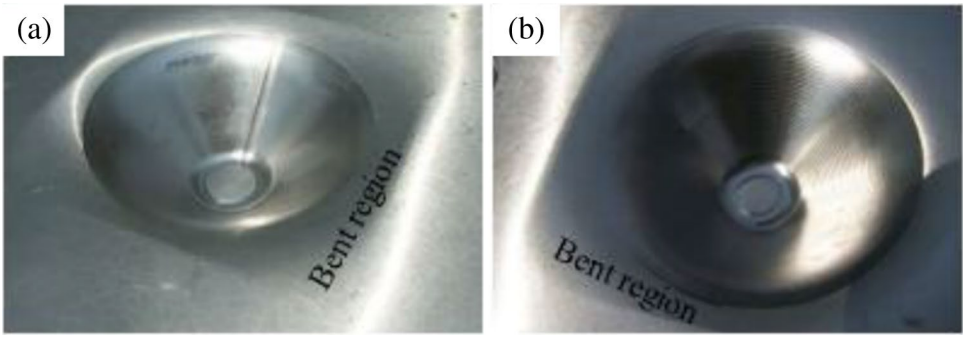

Fig. 19 Products produced by different tool path profiles. **a** Contour, **b** helical [69]

4.2 Compensation and RSM optimisation

The study by Azaouzi and Lebaal [72] created a response surface method (RSM) to optimise the tool path. According to the study, the original tool path was obtained from the FE modelling and optimised by combining the quadratic programming algorithm and surface response method, as shown in Fig. 20. The parameter h and d represent the depth and diameter for the stage 1 tool path, and H and D represent the depth and diameter for the stage 2 tool path. H and D are constants to form designed forming shape, and h and d are design variables to optimise the tool path. The optimised tool path has been applied in simulation to predict the thickness distribution. The results show that the thickness at the maximum depth decreased by approximately 1 mm, and the distribution approaches constant which reduced the tool motion fluctuations. The tool is more fit with low-fluctuated thickness distribution where the risk of crack is reduced and the surface quality is increased; the geometric accuracy is also improved according to optimised tool path. Behera et al. [73] investigated a multi-variate adaptive regression spline (MARS) non-parametric regression analysis to compensate for the tool path inaccuracies of the SPIF process. The study commented that the obtained geometric issues can be captured by graphs, and the framework may study the topological conceptual graphs to predict the optimal tool path. Other studies by [20, 74–78] implemented algorithms to correct the tool path depending on the process parameters to improve the geometric accuracy. Observations have revealed that the tool path correction and compensation are based on the number of parameters affecting the accuracy. The tool path optimisation is efficient in single-parameter calculation and becomes less efficient in calculating the multi-parameter system.

4.3 ANN optimisation and image network analysis

Due to improvements in computing technology, machine learning has been applied in optimising tool paths to improve geometric accuracy. For instance, Liu et al. [24], Akrichi et al. [79] and Li et al. [67] applied the deep learning artificial neural networks (ANN) model to predict the forming parameters, including the construction of tool path plan, calculation of roundness and positioning deviation for each increment step. The ANN tool path optimisation is shown in Fig. 21. The promising results have shown the

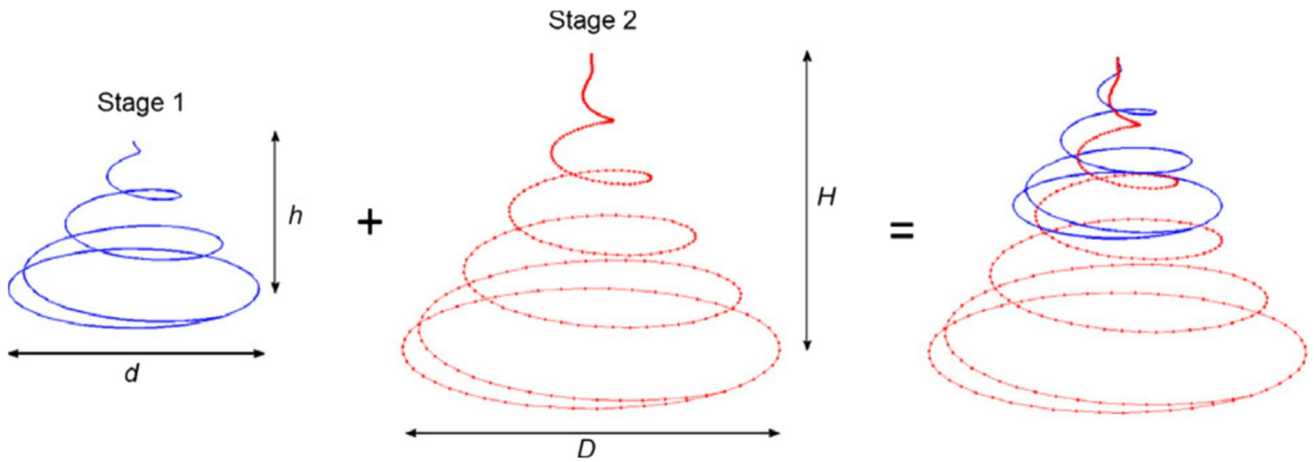

Fig. 20 Tool path optimisation [72]

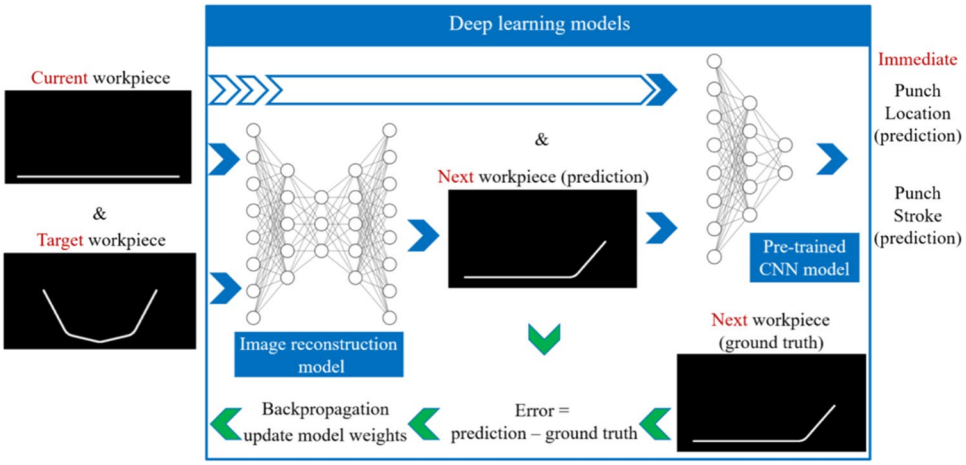

Fig. 21 ANN optimisation process [24]

framework's suitability for complex sheet metal forming to optimise the tool path planning. Jiang et al. [27] proposed the ANN framework's use in electric heating SPIF systems to study the measured temperature and forming force and apply neurons and predict the outcome according to the process parameters. The predicted values can be further used in microstructural revolution, which provides clear evidence that machine learning is applicable in heat-assisted SPIF systems to enhance the process parameters. Furthermore, Behera et al. [76] proposed an image network analysis with the integration of topological conceptual graphs on the critical stages during the process. The outcomes will be studied and optimised by analysing algorithm to compensate the error from the tool path. Furthermore, an optimised tool path will be created to improve the geometric accuracy at critical area during the SPIF process. Similarly, Bautista-Monsalve et al. [80] investigated an image database to make training of different classification algorithms as learning approach to study the wear and cracks on the forming surface to predict the surface quality for heat-assisted SPIF for Ti-6Al-4 V sheets. The image network is efficient for all ISF systems in capturing the forming effects, including the geometric coordinates, thickness distribution and surface quality to optimise the tool path plan, which compensate the error from tool motion, wear and cracks according to the process. However, the performance depends on the efficiency of algorithm in analysing the visual effects, which requires high-resolution image and wide range of capturing. The error percentage is relatively higher than ANN networks on optimisation of obtained parameters.

5 Summary of tool path design

The tool path for ISF operations is significant in producing accurate forming shapes. Process parameters, including step size, feed rate, tool shape and diameter, will affect accuracy. To eliminate the limitations, the tool path can be optimised to compensate for the geometrical from the process parameters to improve the forming accuracy. Table 3 shows the details of the tool design.

6 Lubricants and coating

Graphite grease, machine oil and MoS_2 paste/spray are common lubricants used in SPIF systems. For the heat-assisted SPIF process, the common lubricants remain unsuitable in terms of achieving high surface quality and geometric accuracy. In this section, different types (paste, spray, liquid) of lubricants will be compared to assess their effect on surface quality and geometric accuracy.

6.1 Lubricants and coatings

Lubricants and coatings are significant factors in affecting surface quality for ISF processes. The selection of lubricant or coating depends on the materials, process parameters and temperature. For room temperature SPIF processes, the sheet materials affect the performance of lubricant and coating as the materials have different surface roughness and yield strength significantly affects the forming forces. The tool motion will be affected by high-forming force, and the performance of lubricant or coating will be reduced, which further causes geometric inaccuracy and cracks. For instance, Sornsuwit and Sittisakuljaroen [81] investigated the performance of MoS_2 on SUS 304 and SUS 316L stainless steels and grade 2 titanium (Ti Gr2). The lubricant MoS_2 is a self-mixed paste of MoS_2 powder with petroleum jelly in a ratio of 4:1. The tool diameter is 10 mm, and all workpieces all have 1 mm thickness and have a feed rate of 3140 mm/min for all experiments. The surface quality for each material is shown in Fig. 22, which shows that the lubricant performance deteriorates according to the yield

strength of the materials; Ti Gr2 revealed the worst surface quality on the deforming surface. Figure 23 reveals the formability and surface roughness. It can be observed that Ti Gr2 also revealed the worst formability and surface roughness distribution. However, MoS_2 still represents the best lubricant for Ti Gr2 sheets compared with other lubricants. Hussain et al. [82] proposed different mixing methods for MoS_2 and graphite powders to make different types of lubricants for SPIF for pure titanium sheets. The study designed three types of lubricants where lubricant 1 is the

Table 3 Summary of tool path design

Tool path	Advantages	Limitations
Contour	- Applicable for all types of forming shapes - High formability and complete finish of forming the design	- The step change tool path will remain a distinct mark on the surface - Relatively lower geometric accuracy and surface quality
Helical	- High geometric accuracy and surface quality (non-contour steps)	- Only applicable for axisymmetric forming shapes - Low formability and unable to complete the full forming shape (limited by algorithm)
Compensation and corrections	- Applicable for all types of tool paths - High performance for single-process parameters	- Complex algorithm design - Low efficiency for multi-process parameters
RSM optimisation	- Aids study of explanatory and response variables to optimise the tool path	- Requires proper design of experiments to achieve accurate results
ANN optimisation	- Aids study of one or more response variables to optimise the process parameters - User-friendly software control	- Requires a high-performance computer to train multi-process parameters
Image network analysis	- Using topological conceptual graphs to solve the critical issues - All calculations are based on captured graphs, which reduces the computing time	- Complex algorithm design - Only applicable for specific captured issues

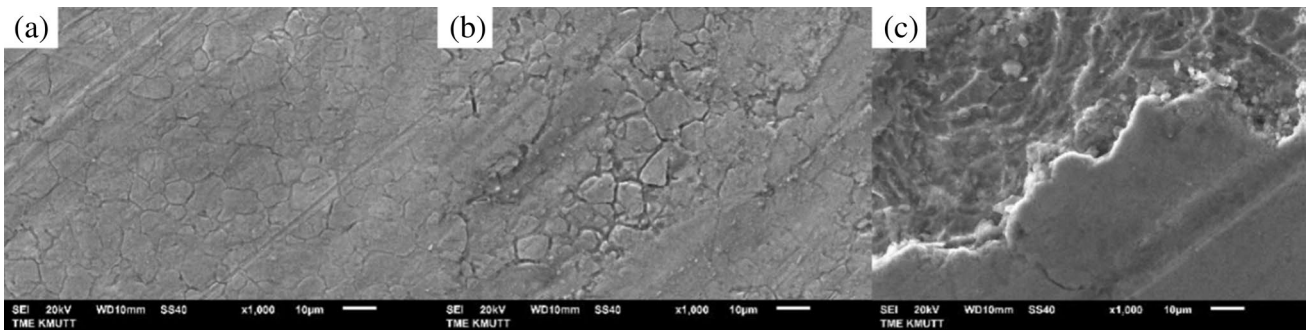

Fig. 22 Surface quality on workpiece. **a** SUS 304, **b** SUS 316L, **c** Ti Gr2 [81]

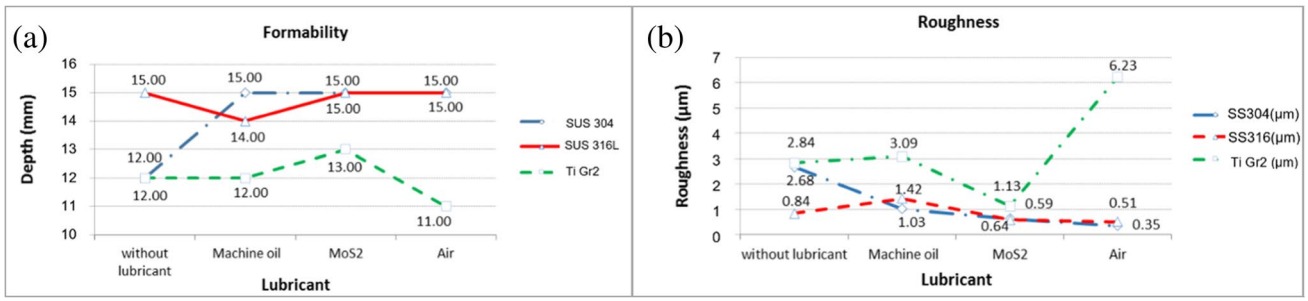

Fig. 23 The effects of formability and surface roughness for different types of lubricant. **a** Formability, **b** surface roughness [81]

liquid type that mixes different percentages of MoS_2 and graphite powders in water, lubricant 2 is paste type which mixes MoS_2 in grease and lubricant 3 is spray type which mixes MoS_2 in alcohol and ketone. According to the results, the spray lubricant indicated an excessive adherence on the surface. The medium paste represents less adherence, and liquid lubricant indicates the lowest adherence and surface roughness, indicating that liquid MoS_2 is more favourable for titanium alloys as there is a low chance of adherence to the deforming surface. Diabb et al. [83] investigated the mixing of SiO_2 nanoparticles in vegetable oil, which revealed the suitability of less viscous liquid lubricant for SPIF processes. Other than the lubricant, Hussain and Al-Ghamdi [84] studied a plasma electrolytic oxidation (PEO) coating comprising MoS_2 powder with electrolyte on workpieces for SPIF processes. The results revealed that the coating on forming surface indicated better performance than the MoS_2 paste with grease, thus representing a better method to improve the surface quality.

For the heat-assisted SPIF process for high-strength materials, the coating was unable to work under elevated temperatures. The conventional lubricants in spray, paste or liquid will dissipate during the process [59, 85]. To improve the lubricating service, Şen et al. [86] have investigated the minimum quantity lubrication (MQL) technique for types of lubricants with different viscosities, which provide a sufficient method to lubricant application to significantly improve the SPIF of HC300LA cold rolled steel sheets. Li et al. [87] developed a mixture lubricant consists of WS_2 powder mixed with high-temperature lubricating oil which successfully reduced the lubricant adherence during 500 °C electric heating–assisted SPIF of Ti-6Al-4 V sheets. Furthermore, Liu et al. [19] developed a water-cooling system on the tool to cool down the ball-roller tool tip and Li et al. [60] improved the design to enable a flow of liquid MoS_2 to lubricate the forming surface and cool down the ball-roller tool tip together. This method able to provide sufficient lubricating to prevent the dissipation and reduce the thermal expansion of tool and contact surface continuously.

6.2 Summary of lubricants and coating

Among the series of lubricants, liquid MoS_2 performed well in ISF processes and this lubricant has been widely used in processing of high-strength alloys such as titanium and steel. The application of lubricant in heat-assisted SPIF process requires a constant existence throughout the process to prevent dissipation during the high-temperature process. The summary of lubricants and coatings are shown in Table 4.

7 Numerical analysis

This section compares different types of numerical analysis (implicit, explicit) in accurately predicting geometric accuracy, thickness distribution, forming force and temperature. Furthermore, the studies of microstructural FE analysis, including CPFEM, RVE and CA, undergo discussion in relation to accurately predicting the microstructure behaviour of SPIF or relevant metal forming processes.

7.1 FE modelling

To predict the mechanical behaviour during the SPIF process, numerical modelling has been established based on user-defined constitutive laws in literature to perform the FE simulation. Currently, commercial ABAQUS, LS-DYNA and ANSYS software provide user-defined processing and post-processing works.

For conventional FE modelling of SPIF works, the tool components are normally considered as a "rigid" body and the sheet materials are defined as "deformable." The movement of the tool in the FE model aligns with the experimental SPIF process, which can be assigned to the path displacements and temperature conditions. The complex forming shape and step size may increase a large number of discrete increments in the simulation. According to Silva and Martins [88], the tolerance setting in the CAM program determined the number of increment points. A tolerance of

Table 4 Summary of application and effects for lubricants and coating

Lubrication	Advantages	Limitations
Spray	- Easy application - Efficient for low-strength materials - Efficient for room temperature SPIF	- Low efficiency for high-strength materials - Not efficient for heat-assisted SPIF
Paste	- Relatively low viscosity - Fast dissipation in heat-assisted SPIF processes	- Low efficiency for high-strength materials - Not efficient for heat-assisted SPIF
Liquid	- Lowest viscosity - High performance for high-strength materials - High performance for heat-assisted SPIF with a water-cooling system	- Must work with a water-cooling system to provide sufficient and sustainable lubrication to the heat-assisted SPIF process
Coating	- High performance for high-strength materials	- Burns-off and removal during heat-assisted SPIF

0.01 mm resulted in approximately 400 increment points per metre for the hyperbolic cone and 8 points per metre (the sides are straight) for the pyramid in the FE simulation. Vertical step down was set equal to 0.5 mm, and the coefficient of friction adopting Amontons–Coulomb's law was assumed to be zero ($\mu = 0$).

To solve a FE problem, certain calculating features and computation time require consideration before running the simulation. For instance, in ABAQUS standard simulation, two solver types, explicit and implicit, are provided to solve FE problems. In the explicit solver, the data output is calculated from the current state; calculation is straightforward, and less computational time is needed for a single explicit increment. However, the solver type is not available for large time increments as the error will increase exponentially and destabilise the calculating method. In the implicit solver, the data output is calculated directly from the previous state, which is a coupled system requiring non-linear algorithms such as the Newton–Raphson method. The computational time and memory required to complete an implicit increment exceed that of an explicit solver because of the number of equations requiring a solution using this method.

In SPIF simulation, the explicit solver tends to consider material quasi-static behaviour to reduce the computational time rather than the implicit solver, which takes more computation time and has a higher risk of producing non-convergence results due to the complex behaviour on tool-workpiece contact. Durgun et al. [89] compared the explicit and implicit solvers in an ABAQUS simulation of SPIF processes. The workpiece has 7300 S4R shell elements and seven thickness elements. Figure 24 shows the geometric and strain comparison between explicit, implicit and optical measurements. According to the findings, both solver types agree with the optical measurement and explicit solver, indicating a relatively better match than the implicit solver. The study also found that the implicit solver has a larger computational time than the explicit solver. However, the explicit solver lacks efficiency for large time increments, as stated by Gupta and Jeswiet [90], which exponentially increased the computational time. The studies [91, 92] proposed that the kinetic energy (ALLKE) must be less than 10% of the maximum internal energy (ALLIE) in the explicit solver. Li et al. [59] investigated the explicit analysis of 600 °C and 700 °C induction heating-assisted SPIF processes for the Ti-6Al-4 V using the C3D8T element. The study proposed a graph to indicate the error and the computational time difference between different mass scaling values, as shown in Fig. 25. Different mass scaling values revealed that lower mass scaling required more computational time, and the percentage of error decreased, as shown in Fig. 25b. Thus, the mass scaling requires controlling to provide higher accuracy and balance the computational time. Desalegn et al. [93] studied the SPIF on different dimensions of geometry and revealed that explicit analysis is more efficient for larger dimensions than small ones. Lora et al. [94] and Ambrogio et al. [95] proposed a combination method using explicit for SPIF operation and implicit for tool release (contact between tool and workpiece), which also saved computational time.

7.2 CPFEM, RVE and CA modelling

Rather than a macroscopic scale analysis of SPIF operations, mesoscopic and microscopic scale analyses can be presented by applying the crystal plasticity finite element method (CPFEM) to simulate the experimental scale or partial scale plasticity behaviour and representative volume element (RVE) to simulate the grain level strain–stress

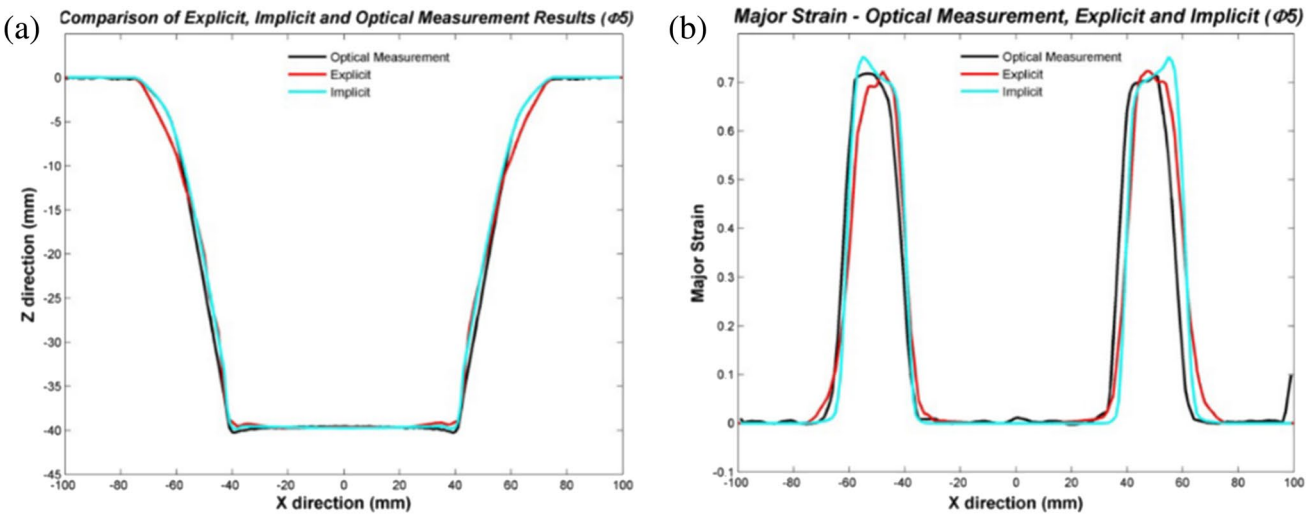

Fig. 24 Geometric and strain comparisons between explicit and implicit analyses [89]

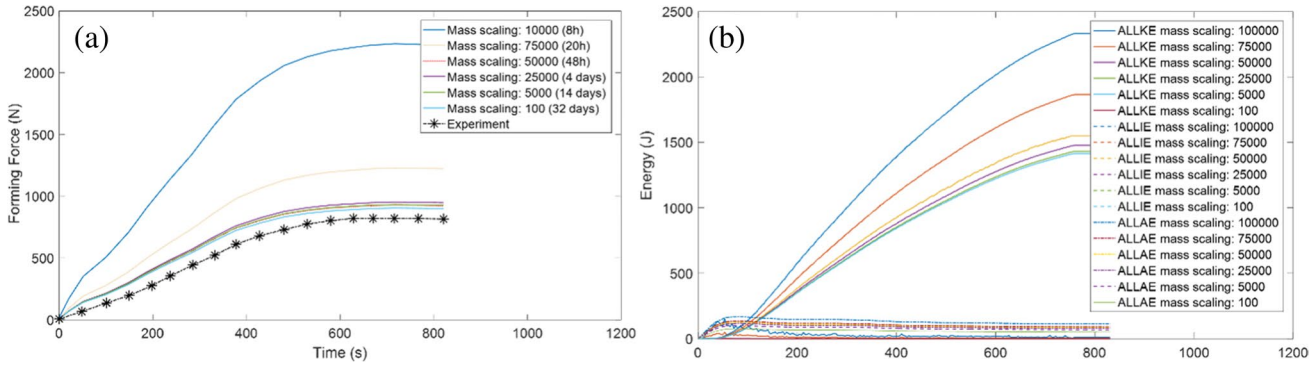

Fig. 25 Effects from different mass scalings. **a** Forming force, **b** energy history [59]

behaviour based on particular parts throughout the process. The studies [96, 97] combined CPFEM and RVE to simulate SPIF of 7075-O aluminium sheet by importing the plasticity properties from CPFEM and used the output results as inputs in the RVE model. Electron backscatter diffraction (EBSD) was used to obtain the grains' orientation at critical parts of the workpiece and established RVE model using DREAM.3D software [98] to present the plasticity behaviour accurately. Han et al. [99] proposed two advanced anisotropic yield functions (Yld2000-2D, Yld2004-18p) to simulate the experimental deep drawing for 2090-T3 aluminium alloy sheets. The output results were compared with experiments, and the best-fit output results were used in RVE model to predict yield surface evolution.

The studies by [100, 101] have applied the Linux coding software DAMASK [102] to establish the auto-generated tessellation to perform microscopic RVE simulation to calculate the grain level orientation, texture and strain–stress behaviour. Based on DAMASK integrated spectral solvers, the calculations on single-crystal constitutive laws can be processed in user-friendly way with less computational time. The studies on numerical framework for CPFEM and RVE [103–105] applied another Linux coding software NEPER [106] to generate auto-generated tessellation or EBSD obtained grains orientation to simulate the DRX and phase-field behaviour on metal processing works. Based on ABAQUS subroutine construction of single-crystal and polycrystal constitutive modelling, the findings indicate that the anisotropy coefficients of materials produced accurate results, and especially for heat-assisted mechanical deformation, anisotropy coefficients depending on temperature must be obtained before simulation. As the software is more flexible to establish and mesh experimental scale model, macroscopic, mesoscopic and microscopic CPFEM and RVE modelling can be formed easily. However, the software did not integrate any solver system; ABAQUS subroutine or other software solving systems have to be used to process the crystal plasticity calculation.

Furthermore, Chuan et al. [107] integrated CPFEM with cellular automata (CA) to demonstrate the dynamic recrystallisation (DRX) for isothermal hot compression, which theoretically validated the combination of crystal plasticity and DRX behaviour to simulate the hot deformation process of steel alloys. Another research Li et al. [108] studied a combining CPFEM, RVE and CA methods to study the grain orientation, crystal texture and DRX for induction heating of SPIF for Ti-6Al-4 V. As shown in Fig. 26. the combination proposed a novel method to study mechanical properties (strain–stress behaviour) in macroscopic scale CPFEM and a transfer of obtained properties to RVE model corresponding to critical forming regions during the process and finally a CA modelling to predict the grains' growth based on obtaining crystal plasticity results from CPFEM and RVE. The process, including extraction of the grain's orientation data from EBSD, applied the information in an experimental scale CPFEM, obtained the grain-level stress–strain data and input the data in RVE to create the crystal texture using the MATLAB toolbox MTEX [109] to produce the DRX behaviour. Single-crystal constitutive models based on general elastic lattice distortion and plastic deformation without effects on lattice geometry were used in the research, and the results were able to output the grain level stress and strain data to form DRX evolution and misorientation angles to form crystal texture. The results were validated with experimental microstructure results. However, the modelling can be improved by inducing phase transition and twin grains calculations to predict the results for temperature up to beta-transus.

7.3 Summary of numerical analysis

The numerical analysis can analyse the mechanical and thermal behaviour for experimental scale SPIF processes, and CPFEM, RVE and CA can estimate the material's microstructure evolution. The comparisons of solver types in FE

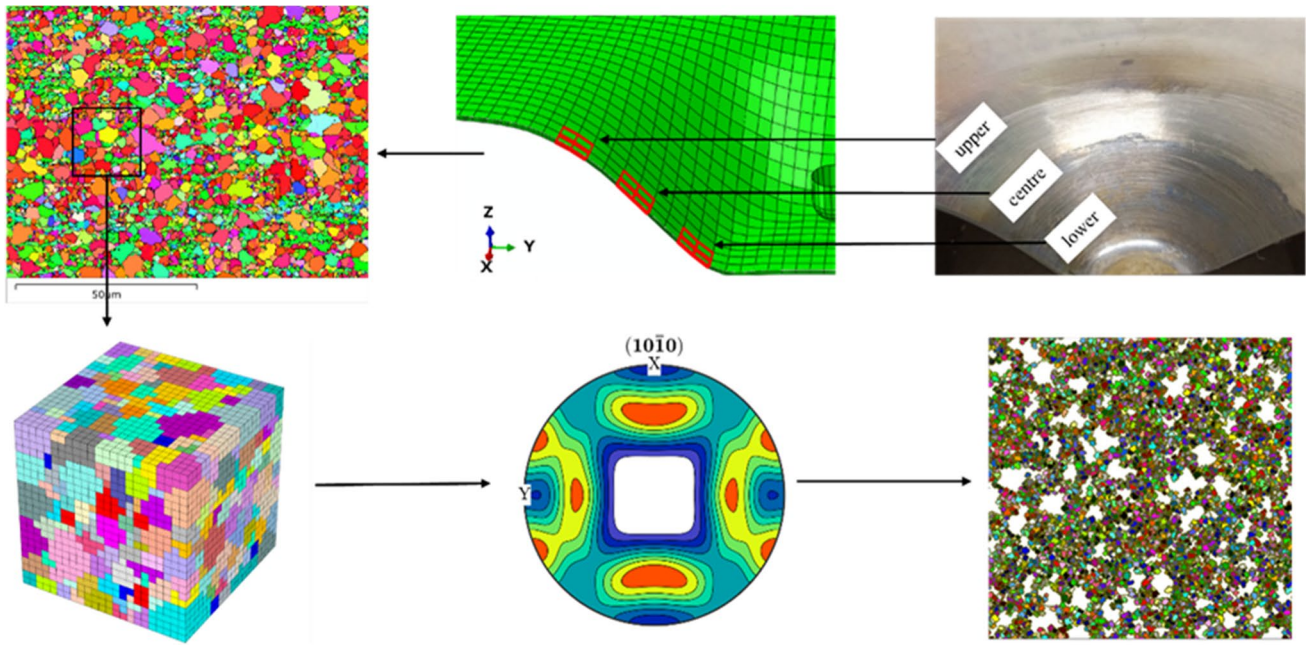

Fig. 26 Process chart for microstructural evolution for heat-assisted SPIF [108]

Table 5 Comparisons of solver types in FE modelling

Solver type	Advantages	Limitations
Explicit	- Low computational time - Efficient for small increment points - Approximately constant increment size	- Not efficient for large increment times - Mass scaling affects the accuracy and computational time
Implicit	- Linear to mildly non-linear - Efficient for large increment times	- Large computational time - Not efficient for small increment times - The accuracy varies for increment size

modelling are presented in Table 5. The summary of FE microstructure analysis is shown in Table 6.

8 Microstructure analysis

This section discusses the effects of microstructural evolution in SPIF room temperature and elevated temperature in correlation with forming force, formability, geometric accuracy, thickness and temperature distribution.

8.1 Microstructure analysis for SPIF

In SPIF process, the tool follows the tool path to make incremental deformation to the sheet materials. The applied forming force and heating induce mechanical and thermal behaviours to the workpiece. The strain hardening work will increase the microstructural evolution, and the domination of such evolution is a critical factor to study to control or optimise the process quality. As shown in Fig. 27, the study by Shrivastava and Tandon [110] revealed the microstructural evolution and grain size distribution in SPIF of AA1050 sheet metals. According to the findings, a strong reduction of grain size can be observed (42.4 to 11.05 μm), which revealed grain refinement throughout the forming process. Furthermore, numerous low angle grain boundaries (2–15 °) have been transformed to high angle boundaries (above 15°), indicating that the work hardening increased.

For heat-assisted SPIF on Ti-6Al-4 V, Li et al. [59] observed pronounced grain refinement for temperatures from as-received to 600 °C and 700 °C as shown in Fig. 28. The study obtained that the increase in temperature successfully increased the ductility of workpiece which reduced the forming force and achieved better geometric accuracy. The study also found that 700 °C induced more DRX initiation than 600 °C which produced finer grain and contributed to the grain boundary strengthening. The grain growth at higher temperature (above 700 °C) is a key factor to produce constant straining work which approached sustainable forming force growth and thus improved the geometric accuracy and remained a stable thickness distribution. Other studies

Table 6 FE microstructure analysis

Solver type	Advantages	Limitations
CPFEM	- Applicable for multi-scale macroscopic, mesoscopic and microscopic scale analyses - Efficient modelling of material's plasticity behaviour	- Polycrystalline model needs more investigation to reduce the consumptions - Single crystal model is constraint for microstructure evolution without phase transition and twin grains
RVE	- Applicable for microscopic scale and mesoscopic scale analyses - Efficient mechanics for heterogeneous materials and plasticity property estimation - Efficient production of grain's level stress, strain and crystal texture	- Not applicable for macroscopic scale analysis - The accuracy varies for increment size
CA	- Applicable for microscopic scale analysis - Efficient for DRX and grain size evolution	- Not applicable for macroscopic scale and mesoscopic scale analyses

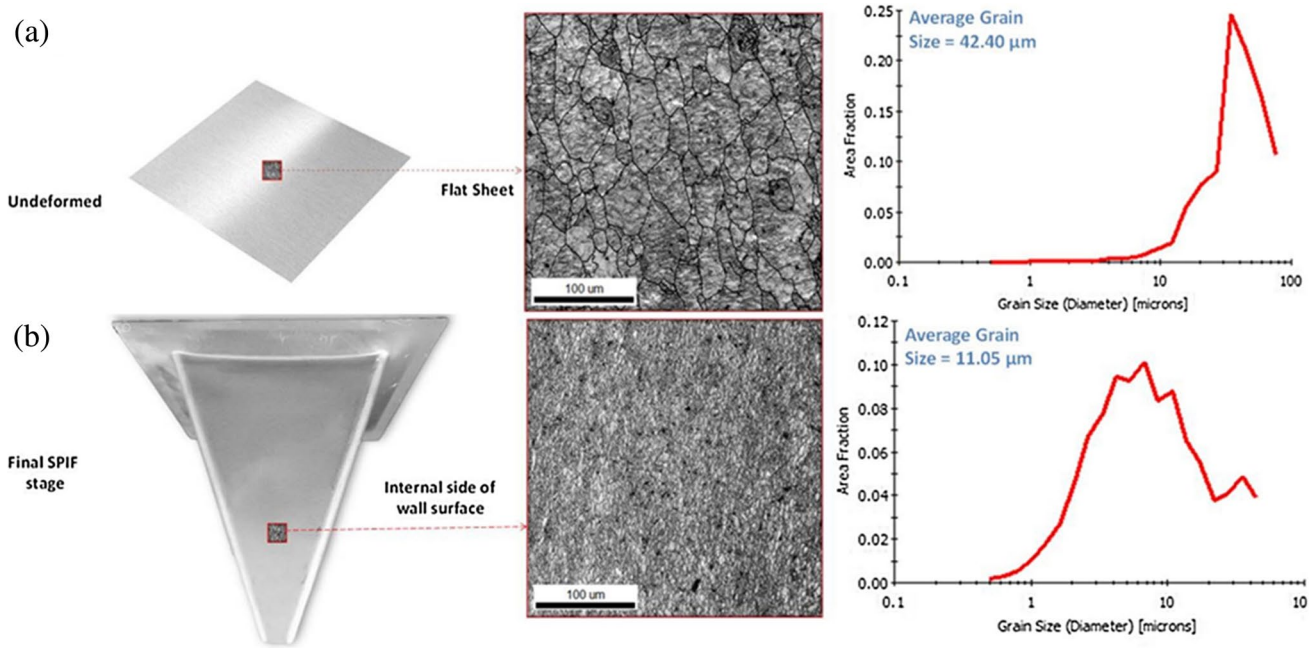

Fig. 27 Microstructural evolution and grain size distribution histogram throughout the SPIF process of AA1050 sheets. **a** As-received sheets, **b** deformed sheets [110]

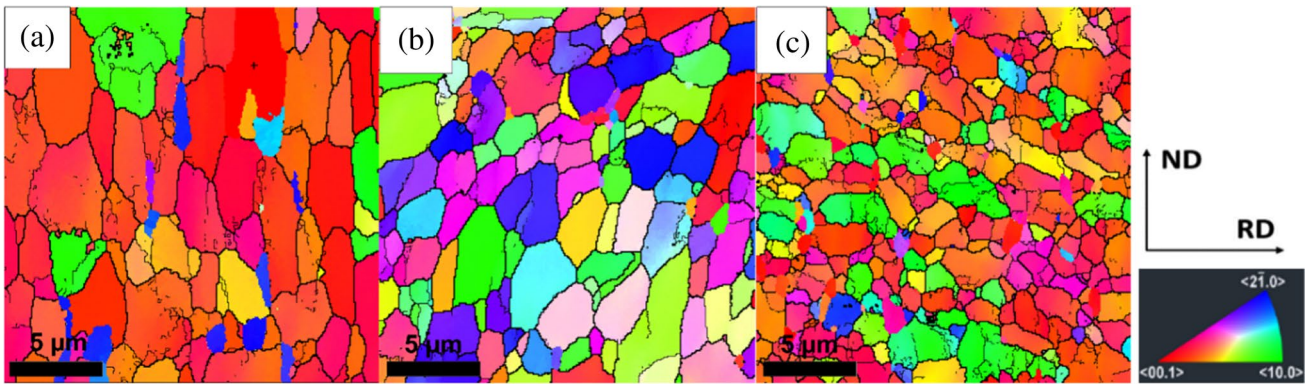

Fig. 28 Microstructural evolution of as-received sample. (a) IPF map of as-received sample, (b) IPF map of 600 °C sample and (c) IPF map of 700 °C sample [59]

by Zhang et al. [111] and Zhang et al. [112] investigated temperature's influence on the formability, microstructure and fracture morphology of SPIF of magnesium materials. The studies revealed that the higher temperature increased the DRX, which reduced the forming force, increased formability and further reduced the risk of fracture. Furthermore, the reduction in grain size activated the grain's boundary dislocation, thus enabling the neighbouring deformation, which enhanced the straining process and achieved higher micro-hardness.

8.2 Summary of microstructure analysis

The microstructure analysis encounters limitations in establishing constitutive models to correlate thermal microstructure evolution and mechanical properties. Unlike measurable mechanical behaviours, the investigation of microstructure can only be obtained from microscopic characteristics on a specific area. For heat-assisted SPIF processes, the unstable forming force and temperature induce different microstructures from starting, centre and ending area. Furthermore, different heating methods and experimental parameters, such as step size, feed rate and tool design, produce a combination of effects to the microstructure evolution. Thus, experimental measured microstructure characteristics should correlate with numerical microstructure analysis by importing the experimental data to the microstructure models to predict the crystal texture, grain orientation and grain size evolution throughout the process. The microstructural analysis is significant to study to produce accurate results to correlate the relationship with mechanical properties.

9 Conclusion

- To apply SPIF on high-strength materials, heat sources can be improved to provide localised temperature to workpiece. The heating temperature should be rapid and moved together with the tool motion to keep constant temperature distribution.
- Ball-roller tools indicate higher formability, surface quality and geometric accuracy than conventional tools. However, the ball roller has a high risk of thermal expansion during high temperature deformation. Thus, water-cooling system is essential to integrate to the tool to provide cooling to the tool and reduce the lubricant dissipation.
- Conventional lubricants and coatings did not provide sufficient performance to the workpiece during heat-assisted SPIF process. High temperature cause rapid dissipation of lubricant and burn-off of coatings. It is essential to design high temperature lubricant to resist the thermo-mechanical behaviour during the SPIF process.
- The helical tool path is preferable for axisymmetric forming shapes, and the contour tool path is preferable for all types of forming shapes. To optimise the tool path plan, RSM, ANN and image analyses can correct and optimise the tool path to compensate for the error from the forming force and temperature. For the heat-assisted SPIF process, ANN has more potential to study the behaviours of temperature and tool path coordinates to produce the optimal tool path. However, the error percentage will increase for unstable temperature distribution.
- Numerical modelling can be correlated with CPFEM, RVE and CA modelling to provide macroscopic-mesoscopic-microstructure analysis throughout the heat-assisted SPIF process. The essential part is to determine accurate experiment and microstructure results and data transfer to the modelling; connection of each model should be studied.

Author contribution Weining Li: conceptualisation, investigation, methodology, validation, formal analysis, writing — original draft. Khamis Essa: writing — review and editing, resources, supervision, project administration. Moataz M Attallah: writing — review and editing, supervision.

Data availability The data included in this study are available upon request by contact with the corresponding author.

Code availability Not applicable.

Declarations

Ethics approval Not applicable.

Consent to participate Not applicable.

Consent for publication Not applicable.

Competing interests The authors declare no competing interests.

References

1. Ham M, Jeswiet J (2006) Single point incremental forming and the forming criteria for AA3003. CIRP Ann 55(1):241–244. https://doi.org/10.1016/S0007-8506(07)60407-7
2. Strano M (2005) Technological representation of forming limits for negative incremental forming of thin aluminum sheets. J Manuf Process 7(2):122–129. https://doi.org/10.1016/s1526-6125(05)70089-x
3. Zhan X, An D, Chen J (2022) A novel two-stage friction stir-assisted incremental sheet forming method for uniform microstructure and enhanced properties in aluminum alloys. Int J Mach Tools Manuf 180:103928. https://doi.org/10.1016/j.ijmachtools.2022.103928
4. Yan Z, Hassanin H, El-Sayed MA, Eldessouky HM, Djuansjah J, Alsaleh NA, Essa K, Ahmadein M (2021) Multistage tool path optimisation of single-point incremental forming process. Materials (Basel) 14(22):6794. https://doi.org/10.3390/ma14226794
5. Davarpanah MA, Mirkouei A, Yu X, Malhotra R, Pilla S (2015) Effects of incremental depth and tool rotation on failure modes and microstructural properties in single point incremental forming of polymers. J Mater Process Technol 222:287–300. https://doi.org/10.1016/j.jmatprotec.2015.03.014
6. Silva MB, Alves LM, Martins PAF (2010) Single point incremental forming of PVC: experimental findings and theoretical interpretation. Eur J Mech A Solids 29(4):557–566. https://doi.org/10.1016/j.euromechsol.2010.03.008
7. Franzen V, Kwiatkowski L, Martins PAF, Tekkaya AE (2009) Single point incremental forming of PVC. J Mater Process Technol 209(1):462–469. https://doi.org/10.1016/j.jmatprotec.2008.02.013
8. Martins PAF, Kwiatkowski L, Franzen V, Tekkaya AE, Kleiner M (2009) Single point incremental forming of polymers. CIRP Ann 58(1):229–232. https://doi.org/10.1016/j.cirp.2009.03.095
9. Jeswiet J, Micari F, Hirt G, Bramley A, Duflou J, Allwood J (2005) Asymmetric single point incremental forming of sheet metal. CIRP Ann 54(2):88–114. https://doi.org/10.1016/s0007-8506(07)60021-3
10. Panjwani D, Priyadarshi S, Jain PK, Samal MK, Roy JJ, Roy D, Tandon P (2017) A novel approach based on flexible supports for forming non-axisymmetric parts in SPISF. Int J Adv Manuf Technol 92(5–8):2463–2477. https://doi.org/10.1007/s00170-017-0223-3
11. Sousa R (2016) Incremental sheet forming technologies, in Reference Module in Materials Science and Materials Engineering. Elsevier. https://doi.org/10.1016/B978-0-12-803581-8.04055-8
12. Ben Said L (2022) The incremental sheet forming; technology, modeling and formability: a brief review. Proc Inst Mech Eng E J Process Mech Eng 236(6): 2729–2755. https://doi.org/10.1177/09544089221093306
13. Liu Z (2018) Heat-assisted incremental sheet forming: a state-of-the-art review. Int J Adv Manuf Technol 98(9–12):2987–3003. https://doi.org/10.1007/s00170-018-2470-3
14. Christopher SHY, Keith AC, James B (2009) Reducing force needed to form a shape from a sheet metal. The Boeing Company, Chicago, IL(US)
15. Lu B, Li Z, Long H, Chen F, Chen J, Ou H (2017) Microstructure refinement by tool rotation-induced vibration in incremental sheet forming. Procedia Engineering 207:795–800. https://doi.org/10.1016/j.proeng.2017.10.831
16. Al-Obaidi A, Kräusel V, Landgrebe D (2016) Hot single-point incremental forming assisted by induction heating. Int J Adv Manuf Technol 82(5):1163–1171. https://doi.org/10.1007/s00170-015-7439-x
17. Göttmann A, Bailly D, Bergweiler G, Bambach M, Stollenwerk J, Hirt G, Loosen P (2012) A novel approach for temperature control in ISF supported by laser and resistance heating. Int J Adv Manuf Technol 67(9–12):2195–2205. https://doi.org/10.1007/s00170-012-4640-z
18. Odenberger EL, Oldenburg M, Thilderkvist P, Stoehr T, Lechler J, Merklein M (2011) Tool development based on modelling and simulation of hot sheet metal forming of Ti–6Al–4V titanium alloy. J Mater Process Technol 211(8):1324–1335. https://doi.org/10.1016/j.jmatprotec.2011.03.001
19. Liu R, Lu B, Xu D, Chen J, Chen F, Ou H, Long H (2016) Development of novel tools for electricity-assisted incremental sheet forming of titanium alloy. Int J Adv Manuf Technol 85(5):1137–1144. https://doi.org/10.1007/s00170-015-8011-4
20. Rauch M, Hascoet J-Y, Hamann J-C, Plenel Y (2009) Tool path programming optimization for incremental sheet forming applications. Comput Aided Des 41(12):877–885. https://doi.org/10.1016/j.cad.2009.06.006
21. Asgar J, Lingam R, Reddy V (2013) Tool path influence on electric pulse aided deformation during incremental sheet metal forming. In: AIP Conference Proceedings. AIP
22. Hussain G, Gao L (2007) A novel method to test the thinning limits of sheet metals in negative incremental forming. Int J Mach Tools Manuf 47(3–4):419–435. https://doi.org/10.1016/j.ijmachtools.2006.06.015
23. Ortiz M, Penalva M, Iriondo E, López de Lacalle LN (2019) Accuracy and surface quality improvements in the manufacturing of Ti-6Al-4V parts using hot single point incremental forming. Metals 9(6):697. https://doi.org/10.3390/met9060697
24. Liu S, Xia Y, Liu Y, Shi Z, Yu H, Li Z, Lin J (2022) Tool path planning of consecutive free-form sheet metal stamping with deep learning. J Mater Process Technol 303:117530. https://doi.org/10.1016/j.jmatprotec.2022.117530
25. Wang C, He A, Weegink KJ, Liu S, Meehan PA (2020) 3D surface representation and trajectory optimization with a learning-based adaptive model predictive controller in incremental forming. J Manuf Process 58:796–810. https://doi.org/10.1016/j.jmapro.2020.08.062
26. Najm SM, Paniti I (2021) Artificial neural network for modeling and investigating the effects of forming tool characteristics on the accuracy and formability of thin aluminum alloy blanks when using SPIF. Int J Adv Manuf Technol 114(9–10):2591–2615. https://doi.org/10.1007/s00170-021-06712-4
27. Jiang Z, Ehmann KF, Cao J (2022) Prediction of forming temperature in electrically-assisted double-sided incremental forming using a neural network. J Mater Process Technol 302:117486. https://doi.org/10.1016/j.jmatprotec.2021.117486
28. Giuseppina A, Claudio C, Luigino F, Francesco G (2016) Theoretical model for temperature prediction in incremental sheet forming – experimental validation. Int J Mech Sci 108–109:39–48. https://doi.org/10.1016/j.ijmecsci.2016.01.030
29. Liu Z (2017) Friction stir incremental forming of AA7075-O sheets: investigation on process feasibility. Procedia Eng 207:783–788. https://doi.org/10.1016/j.proeng.2017.10.829
30. Grün PA, Uheida EH, Lachmann L, Dimitrov D, Oosthuizen GA (2018) Formability of titanium alloy sheets by friction stir incremental forming. Int J Adv Manuf Technol 99(5–8):1993–2003. https://doi.org/10.1007/s00170-018-2541-5
31. Ambrogio G, Gagliardi F (2014) Temperature variation during high speed incremental forming on different lightweight alloys. Int J Adv Manuf Technol 76(9–12):1819–1825. https://doi.org/10.1007/s00170-014-6398-y
32. Jimma T, Kasuga Y, Iwaki N, Miyazawa O, Mori E, Ito K, Hatano H (1998) An application of ultrasonic vibration to the deep drawing process. J Mater Process Technol 80–81:406–412. https://doi.org/10.1016/s0924-0136(98)00195-2

33. Murakawa M, Jin M (2001) The utility of radially and ultrasonically vibrated dies in the wire drawing process. J Mater Process Technol 113(1–3):81–86. https://doi.org/10.1016/s0924-0136(01)00635-5
34. Baghlani V, Mehbudi P, Akbari J, Sohrabi M (2013) Ultrasonic assisted deep drilling of Inconel 738LC superalloy. Procedia CIRP 6:571–576. https://doi.org/10.1016/j.procir.2013.03.096
35. Shen X-H, Zhang J, Xing DX, Zhao Y (2011) A study of surface roughness variation in ultrasonic vibration-assisted milling. Int J Adv Manuf Technol 58(5–8):553–561. https://doi.org/10.1007/s00170-011-3399-y
36. Mousavi SAAA, Feizi H, Madoliat R (2007) Investigations on the effects of ultrasonic vibrations in the extrusion process. J Mater Process Technol 187–188:657–661. https://doi.org/10.1016/j.jmatprotec.2006.11.168
37. Bagudanch I, Garcia-Romeu ML, Centeno G, Elías-Zúñiga A, Ciurana J (2015) Forming force and temperature effects on single point incremental forming of polyvinylchloride. J Mater Process Technol 219:221–229. https://doi.org/10.1016/j.jmatprotec.2014.12.004
38. Sharma M, Gupta VK, Tandon P (2022) Numerical analysis of the effects of ultrasonic vibrations and elevated temperature in incremental sheet forming. Proc Inst Mech Eng C J Mech Eng Sci 09544062221085907. https://doi.org/10.1177/09544062221085907
39. Sakhtemanian MR, Honarpisheh M, Amini S (2019) A novel material modeling technique in the single-point incremental forming assisted by the ultrasonic vibration of low carbon steel/commercially pure titanium bimetal sheet. Int J Adv Manuf Technol 102(1–4):473–486. https://doi.org/10.1007/s00170-018-3148-6
40. Cheng R, Wiley N, Short M, Liu X, Taub A (2019) Applying ultrasonic vibration during single-point and two-point incremental sheet forming. Procedia Manuf 34:186–192. https://doi.org/10.1016/j.promfg.2019.06.137
41. Bai L, Li Y, Yang M, Lin Y, Yuan Q, Zhao R (2019) Modeling and analysis of single point incremental forming force with static pressure support and ultrasonic vibration. Materials (Basel) 12(12). https://doi.org/10.3390/ma12121899
42. Sun Y, Lu Z, Li C, Wang R, Zhai W (2021) Study on the springback effect and surface property for ultrasonic-assisted incremental sheet forming of aluminum alloy. Symmetry 13(7). https://doi.org/10.3390/sym13071217
43. Cheng Z, Li Y, Li J, Li F, Meehan PA (2022) Ultrasonic assisted incremental sheet forming: constitutive modeling and deformation analysis. J Mater Process Technol 299:117365. https://doi.org/10.1016/j.jmatprotec.2021.117365
44. Li Z, Lu S, Zhang T, Zhang C, Mao Z (2018) Electric assistance hot incremental sheet forming: an integral heating design. Int J Adv Manuf Technol 96(9–12):3209–3215. https://doi.org/10.1007/s00170-018-1792-5
45. Magnus CS (2016) Joule heating of the forming zone in incremental sheet metal forming: Part 1. Int J Adv Manuf Technol 91(1–4):1309–1319. https://doi.org/10.1007/s00170-016-9786-7
46. Min J, Seim P, Störkle D, Thyssen L, Kuhlenkötter B (2016) Thermal modeling in electricity assisted incremental sheet forming. Int J Mater Form 10(5):729–739. https://doi.org/10.1007/s12289-016-1315-6
47. Meier H, Magnus C (2013) Incremental sheet metal forming with direct resistance heating using two moving tools. Key Eng Mater 554–557:1362–1367. https://doi.org/10.4028/www.scientific.net/KEM.554-557.1362
48. Möllensiep D, Kulessa P, Thyssen L, Kuhlenkötter B (2020) Regression-based compensation of part inaccuracies in incremental sheet forming at elevated temperatures. Int J Adv Manuf Technol 109(7–8):1917–1928. https://doi.org/10.1007/s00170-020-05625-y
49. Fan G, Gao L, Hussain G, Wu Z (2008) Electric hot incremental forming: a novel technique. Int J Mach Tools Manuf 48(15):1688–1692. https://doi.org/10.1016/j.ijmachtools.2008.07.010
50. Vahdani M, Mirnia MJ, Gorji H, Bakhshi-Jooybari M (2019) Experimental investigation of formability and surface finish into resistance single-point incremental forming of Ti–6Al–4V titanium alloy using Taguchi design. Trans Indian Inst Met 72(4):1031–1041. https://doi.org/10.1007/s12666-019-01577-4
51. Fan G, Sun F, Meng X, Gao L, Tong G (2009) Electric hot incremental forming of Ti-6Al-4V titanium sheet. Int J Adv Manuf Technol 49(9–12):941–947. https://doi.org/10.1007/s00170-009-2472-2
52. Ao D, Gao J, Chu X, Lin S, Lin J (2020) Formability and deformation mechanism of Ti-6Al-4V sheet under electropulsing assisted incremental forming. Int J Solids Struct 202:357–367. https://doi.org/10.1016/j.ijsolstr.2020.06.028
53. Vahdani M, Mirnia MJ, Bakhshi-Jooybari M, Gorji H (2019) Electric hot incremental sheet forming of Ti-6Al-4V titanium, AA6061 aluminum, and DC01 steel sheets. Int J Adv Manuf Technol 103(1–4):1199–1209. https://doi.org/10.1007/s00170-019-03624-2
54. Duflou JR, Callebaut B, Verbert J, De Baerdemaeker H (2007) Laser assisted incremental forming: formability and accuracy improvement. CIRP Ann 56(1):273–276. https://doi.org/10.1016/j.cirp.2007.05.063
55. Lehtinen P, Väisänen T, Salmi M (2015) The effect of local heating by laser irradiation for aluminum, deep drawing steel and copper sheets in incremental sheet forming. Phys Procedia 78:312–319. https://doi.org/10.1016/j.phpro.2015.11.045
56. Göttmann A, Diettrich J, Bergweiler G, Bambach M, Hirt G, Loosen P, Poprawe R (2011) Laser-assisted asymmetric incremental sheet forming of titanium sheet metal parts. Prod Eng Res Devel 5(3):263–271. https://doi.org/10.1007/s11740-011-0299-9
57. Al-Obaidi A, Kräusel V, Landgrebe D (2017) Induction heating validation of dieless single-point incremental forming of AHSS. J Manuf Mater Process 1. https://doi.org/10.3390/jmmp1010005
58. Ambrogio G, Gagliardi F, Chamanfar A, Misiolek WZ, Filice L (2017) Induction heating and cryogenic cooling in single point incremental forming of Ti-6Al-4V: process setup and evolution of microstructure and mechanical properties. Int J Adv Manuf Technol 91(1):803–812. https://doi.org/10.1007/s00170-016-9794-7
59. Li W, Attallah MM, Essa K (2022) Experimental and numerical investigations on the process quality and microstructure during induction heating assisted incremental forming of Ti-6Al-4V sheet. J Mater Process Technol 299:117323. https://doi.org/10.1016/j.jmatprotec.2021.117323
60. Li W, Essa K, Li S (2022) A novel tool to enhance the lubricant efficiency on induction heat-assisted incremental sheet forming of Ti-6Al-4V sheets. Int J Adv Manuf Technol. https://doi.org/10.1007/s00170-022-09284-z
61. Jeswiet J, Adams D, Doolan M, McAnulty T, Gupta P (2015) Single point and asymmetric incremental forming. Adv Manuf 3(4):253–262. https://doi.org/10.1007/s40436-015-0126-1
62. Kumar A, Gulati V, Kumar P, Singh V, Kumar B, Singh H (2019) Parametric effects on formability of AA2024-O aluminum alloy sheets in single point incremental forming. J Market Res 8(1):1461–1469. https://doi.org/10.1016/j.jmrt.2018.11.001
63. Iseki H (2001) An approximate deformation analysis and FEM analysis for the incremental bulging of sheet metal using a spherical roller. J Mater Process Technol 111(1–3):150–154. https://doi.org/10.1016/s0924-0136(01)00500-3

64. Iseki H, Naganawa T (2002) Vertical wall surface forming of rectangular shell using multistage incremental forming with spherical and cylindrical rollers. J Mater Process Technol 130–131:675–679. https://doi.org/10.1016/s0924-0136(02)00735-5
65. Lu B, Fang Y, Xu DK, Chen J, Ou H, Moser NH, Cao J (2014) Mechanism investigation of friction-related effects in single point incremental forming using a developed oblique roller-ball tool. Int J Mach Tools Manuf 85:14–29. https://doi.org/10.1016/j.ijmachtools.2014.04.007
66. Naranjo JA, Miguel V, Coello J, Manjabacas MC, Martinez-Martinez A, Garcia-Martinez E (2021) Tribological characterization of the heat-assisted single point incremental forming process applied to the Ti6Al4V alloy with the definition of an adhesion parameter for the tool surface. Materials (Basel) 14(24):7641. https://doi.org/10.3390/ma14247641
67. Li W, Shu C, Hassan A, Attallah MM, Essa K (2022) Application of machine learning on tool path optimisation and cooling lubricant in induction heating-assisted single point incremental sheet forming of Ti-6Al-4V sheets. Int J Adv Manuf Technol. https://doi.org/10.1007/s00170-022-10213-3
68. Suresh K, Khan A, Regalla SP (2013) Tool path definition for numerical simulation of single point incremental forming. Procedia Eng 64:536–545. https://doi.org/10.1016/j.proeng.2013.09.128
69. Reddy NV, Lingam R, Cao J (2015) Incremental metal forming processes in manufacturing. In: Handbook of manufacturing engineering and technology 411–452. https://doi.org/10.1007/978-1-4471-4670-4_45
70. Skjoedt M, Hancock MH, Bay N (2007) Creating helical tool paths for single point incremental forming. Key Eng Mater 344:583–590. https://doi.org/10.4028/www.scientific.net/KEM.344.583
71. Attanasio A, Ceretti E, Giardini C, Mazzoni L (2008) Asymmetric two points incremental forming: improving surface quality and geometric accuracy by tool path optimization. J Mater Process Technol 197(1–3):59–67. https://doi.org/10.1016/j.jmatprotec.2007.05.053
72. Azaouzi M, Lebaal N (2012) Tool path optimization for single point incremental sheet forming using response surface method. Simul Model Pract Theory 24:49–58. https://doi.org/10.1016/j.simpat.2012.01.008
73. Behera AK, Verbert J, Lauwers B, Duflou JR (2013) Tool path compensation strategies for single point incremental sheet forming using multivariate adaptive regression splines. Comput Aided Des 45(3):575–590. https://doi.org/10.1016/j.cad.2012.10.045
74. Praveen K, Lingam R, Venkata Reddy N (2020) Tool path design system to enhance accuracy during double sided incremental forming: an analytical model to predict compensations for small/large components. J Manuf Process 58:510–523. https://doi.org/10.1016/j.jmapro.2020.08.014
75. Fu Z, Mo J, Han F, Gong P (2012) Tool path correction algorithm for single-point incremental forming of sheet metal. Int J Adv Manuf Technol 64(9–12):1239–1248. https://doi.org/10.1007/s00170-012-4082-7
76. Behera AK, Lauwers B, Duflou JR (2014) Tool path generation framework for accurate manufacture of complex 3D sheet metal parts using single point incremental forming. Comput Ind 65(4):563–584. https://doi.org/10.1016/j.compind.2014.01.002
77. Nasulea D, Oancea G (2018) Integrating a new software tool used for tool path generation in the numerical simulation of incremental forming processes. Strojniški vestnik - J Mech Eng 64(10):643–651. https://doi.org/10.5545/sv-jme.2018.5475
78. Dittrich M-A, Uhlich F, Denkena B (2019) Self-optimizing tool path generation for 5-axis machining processes. CIRP J Manuf Sci Technol 24:49–54. https://doi.org/10.1016/j.cirpj.2018.11.005
79. Akrichi S, Abbassi A, Abid S, Ben Yahia N (2019) Roundness and positioning deviation prediction in single point incremental forming using deep learning approaches. Adv Mech Eng 11(7):1687814019864465. https://doi.org/10.1177/1687814019864465
80. Bautista-Monsalve F, García-Sevilla F, Miguel V, Naranjo J, Manjabacas MC (2021) A novel machine-learning-based procedure to determine the surface finish quality of titanium alloy parts obtained by heat assisted single point incremental forming. Metals 11(8):1287. https://doi.org/10.3390/met11081287
81. Sornsuwit N, Sittisakuljaroen S (2014) The effect of lubricants and material properties in surface roughness and formability for single point incremental forming process. Adv Mater Res 979:359–362. https://doi.org/10.4028/www.scientific.net/AMR.979.359
82. Hussain G, Gao L, Hayat N, Cui Z, Pang YC, Dar NU (2008) Tool and lubrication for negative incremental forming of a commercially pure titanium sheet. J Mater Process Technol 203(1–3):193–201. https://doi.org/10.1016/j.jmatprotec.2007.10.043
83. Diabb J, Rodríguez CA, Mamidi N, Sandoval JA, Taha-Tijerina J, Martínez-Romero O, Elías-Zúñiga A (2017) Study of lubrication and wear in single point incremental sheet forming (SPIF) process using vegetable oil nanolubricants. Wear 376–377:777–785. https://doi.org/10.1016/j.wear.2017.01.045
84. Hussain G, Al-Ghamdi KA (2014) PEO coating as lubrication means for SPIF of titanium sheet: characteristics and performance. Mater Res Innov 18(sup2):S2-727-S2-733. https://doi.org/10.1179/1432891714z.000000000504
85. Azevedo NG, Farias JS, Bastos RP, Teixeira P, Davim JP, Alves de Sousa RJ (2015) Lubrication aspects during single point incremental forming for steel and aluminum materials. Int J Precis Eng Manuf 16(3):589–595. https://doi.org/10.1007/s12541-015-0079-0
86. Şen N, Şirin Ş, Kıvak T, Civek T, Seçgin Ö (2022) A new lubrication approach in the SPIF process: evaluation of the applicability and tribological performance of MQL. Tribol Int 171:107546. https://doi.org/10.1016/j.triboint.2022.107546
87. Li Z, He S, Zhang Y, Gao Z, An Z, Lu S (2022) A novel current-carrying lubrication in electric hot incremental forming of Ti–6Al–4V titanium sheet. J Braz Soc Mech Sci Eng 44(5):216. https://doi.org/10.1007/s40430-022-03485-z
88. Silva MB, Martins PAF (2014) Incremental sheet forming. In: Hashmi S et al (eds) Comprehensive materials processing. Elsevier, Oxford, pp 7–26
89. Durgun I, Tamer E, Özdemir İ, Baranoğlu B, Sakin A, Music O (2013) Simulation for incremental sheet forming process: a comparison of implicit and explicit finite element analysis with experimental data. 7th International Conference and Exhibition on Design and Production of MACHINES and DIES/MOLDS. Antalya, Turkey
90. Gupta P, Jeswiet J (2019) Parameters for the FEA simulations of single point incremental forming. Product Manuf Res 7(1):161–177. https://doi.org/10.1080/21693277.2019.1608330
91. Essa K, Hartley P (2010) An assessment of various process strategies for improving precision in single point incremental forming. IntJ Mater Form 4(4):401–412. https://doi.org/10.1007/s12289-010-1004-9
92. Essa K, Hartley P (2009) Numerical simulation of single and dual pass conventional spinning processes. Int J Mater Form 2(4):271–281. https://doi.org/10.1007/s12289-009-0602-x
93. Desalegn D, Ramulu PJ, Hailu D, Kumaran SS, Velmurugan P, Venkateswarlu D (2019) Formability analyses on single point incremental sheet forming process on aluminum 1050. Mater Sci Forum 969:703–708. https://doi.org/10.4028/www.scientific.net/MSF.969.703

94. Lora FA, Boff U, Yurgel CC, Folle LF, Schaeffer L (2013) Validation of the computer simulation process applied to the incremental forming process for the evaluation of strain paths. Key Eng Mater 554–557:2453–2461. https://doi.org/10.4028/www.scientific.net/KEM.554-557.2453
95. Ambrogio G, Filice L, Fratini L, Ingarao G, Manco L (2007) Measuring of geometrical precision of some parts obtained by asymmetric incremental forming process after trimming. AIP Conf Proc 908(1):431–436. https://doi.org/10.1063/1.2740849
96. Esmaeilpour R, Kim H, Park T, Pourboghrat F, Xu Z, Mohammed B, Abu-Farha F (2018) Calibration of Barlat Yld 2004–18P yield function using CPFEM and 3D RVE for the simulation of single point incremental forming (SPIF) of 7075-O aluminum sheet. Int J Mech Sci 145:24–41. https://doi.org/10.1016/j.ijmecsci.2018.05.015
97. Esmaeilpour R, Kim H, Asgharzadeh A, NazariTiji SA, Pourboghrat F, Banu M, Bansal A, Taub A (2021) Experimental validation of the simulation of single-point incremental forming of AA7075 sheet with Yld 2004–18P yield function calibrated with crystal plasticity model. Int J Adv Manuf Technol 113(7–8):2031–2047. https://doi.org/10.1007/s00170-021-06706-2
98. Groeber MA, Jackson MA (2014) DREAM.3D: a digital representation environment for the analysis of microstructure in 3D. Integr Mater Manuf Innov 3(1):56–72. https://doi.org/10.1186/2193-9772-3-5
99. Han F, Diehl M, Roters F, Raabe D (2020) Using spectral-based representative volume element crystal plasticity simulations to predict yield surface evolution during large scale forming simulations. J Mater Process Technol 277:116449. https://doi.org/10.1016/j.jmatprotec.2019.116449
100. Hansen LT, Fullwood DT, Homer ER, Wagoner RH, Lim H, Carroll JD, Zhou G, Bong HJ (2020) An investigation of geometrically necessary dislocations and back stress in large grained tantalum via EBSD and CPFEM. Mater Sci Eng A 772:138704. https://doi.org/10.1016/j.msea.2019.138704
101. Li W, Wang L, Zhou B, Liu C, Zeng X (2019) Grain-scale deformation in a Mg−0.8 wt% Y alloy using crystal plasticity finite element method. J Mater Sci Technol 35(10):2200–2206. https://doi.org/10.1016/j.jmst.2019.04.030
102. Raabe D, Roters F (2019) DAMASK – Duesseldorf Advanced Material Simulation Kit for multi-physics phenomena. Comput Mater Sci 158:420–478
103. Ruiz Sarrazola DA, Pino Muñoz D, Bernacki M (2020) A new numerical framework for the full field modeling of dynamic recrystallization in a CPFEM context. Comput Mater Sci 179:109645. https://doi.org/10.1016/j.commatsci.2020.109645
104. Zhang J, Li X, Xu D, Teng C, Wang H, Yang L, Ju H, Xu H, Meng Z, Ma Y, Wang Y, Yang R (2021) Phase field simulation of the stress-induced α microstructure in Ti–6Al–4V alloy and its CPFEM properties evaluation. J Mater Sci Technol 90:168–182. https://doi.org/10.1016/j.jmst.2020.12.085
105. Sedighiani K, Diehl M, Traka K, Roters F, Sietsma J, Raabe D (2020) An efficient and robust approach to determine material parameters of crystal plasticity constitutive laws from macro-scale stress–strain curves. Int J Plast 134:102779. https://doi.org/10.1016/j.ijplas.2020.102779
106. Quey R, Dawson PR, Barbe F (2011) Large-scale 3D random polycrystals for the finite element method: generation, meshing and remeshing. Comput Methods Appl Mech Eng 200(17–20):1729–1745. https://doi.org/10.1016/j.cma.2011.01.002
107. Chuan W, He Y, Wei LH (2013) Modeling of discontinuous dynamic recrystallization of a near-α titanium alloy IMI834 during isothermal hot compression by combining a cellular automaton model with a crystal plasticity finite element method. Comput Mater Sci 79:944–959. https://doi.org/10.1016/j.commatsci.2013.08.004
108. Li W, Li S, Li X, Xu D, Shao Y, Attallah MM, Essa K (2022) Crystal plasticity model of induction heating-assisted incremental sheet forming with recrystallisation simulation in cellular automata. Int J Adv Manuf Technol. https://doi.org/10.1007/s00170-022-10203-5
109. Niessen F, Nyyssonen T, Gazder AA, Hielscher R (2022) Parent grain reconstruction from partially or fully transformed microstructures in MTEX. J Appl Crystallogr 55(Pt 1):180–194. https://doi.org/10.1107/S1600576721011560
110. Shrivastava P, Tandon P (2019) Microstructure and texture based analysis of forming behavior and deformation mechanism of AA1050 sheet during single point incremental forming. J Mater Process Technol 266:292–310. https://doi.org/10.1016/j.jmatprotec.2018.11.012
111. Zhang H, Chu X, Lin S, Bai H, Sun J (2021) Temperature influence on formability and microstructure of AZ31B during electric hot temperature-controlled incremental forming. Materials (Basel) 14(4):810. https://doi.org/10.3390/ma14040810
112. Zhang S, Tang GH, Shen JD, Li Z, Jiang XK (2021) Influence of forming temperature on microstructure and fracture morphology of magnesium alloy during warm incremental sheet forming. Suxing Gongcheng Xuebao/J Plast Eng 28(3):84–91. https://doi.org/10.3969/j.issn.1007-2012.2021.03.011